

**NUCLEAR DATA AND MEASUREMENTS SERIES**

**ANL/NDM-2  
Prompt Air-Scattering Corrections  
for a Fast-Neutron Fission Detector:  $E_n \leq 5$  MeV**

by

Donald L. Smith

September 1973

**ARGONNE NATIONAL LABORATORY,  
ARGONNE, ILLINOIS 60439, U.S.A.**

# NUCLEAR DATA AND MEASUREMENTS SERIES

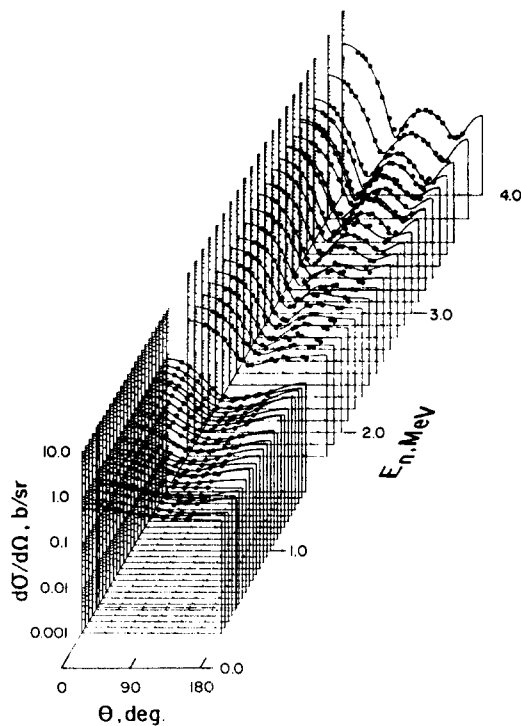
ANL/NDM-2

PROMPT AIR-SCATTERING CORRECTIONS FOR A  
FAST-NEUTRON FISSION DETECTOR:  $E_n \leq 5 \text{ MeV}$

by

Donald L. Smith

September 1973



ARGONNE NATIONAL LABORATORY,  
ARGONNE, ILLINOIS 60439, U.S.A.

The facilities of Argonne National Laboratory are owned by the United States Government. Under the terms of a contract (W-31-109-Eng-38) between the U. S. Atomic Energy Commission, Argonne Universities Association and The University of Chicago, the University employs the staff and operates the Laboratory in accordance with policies and programs formulated, approved and reviewed by the Association.

#### MEMBERS OF ARGONNE UNIVERSITIES ASSOCIATION

The University of Arizona	Kansas State University	The Ohio State University
Carnegie-Mellon University	The University of Kansas	Ohio University
Case Western Reserve University	Loyola University	The Pennsylvania State University
The University of Chicago	Marquette University	Purdue University
University of Cincinnati	Michigan State University	Saint Louis University
Illinois Institute of Technology	The University of Michigan	Southern Illinois University
University of Illinois	University of Minnesota	The University of Texas at Austin
Indiana University	University of Missouri	Washington University
Iowa State University	Northwestern University	Wayne State University
The University of Iowa	University of Notre Dame	The University of Wisconsin

#### NOTICE

This report was prepared as an account of work sponsored by the United States Government. Neither the United States nor the United States Atomic Energy Commission, nor any of their employees, nor any of their contractors, subcontractors, or their employees, makes any warranty, express or implied, or assumes any legal liability or responsibility for the accuracy, completeness or usefulness of any information, apparatus, product or process disclosed, or represents that its use would not infringe privately-owned rights.

ANL/NDM-2

PROMPT AIR-SCATTERING CORRECTIONS FOR A  
FAST-NEUTRON FISSION DETECTOR:  $E_n \leq 5 \text{ MeV}$

by

Donald L. Smith

September 1973

Applied Physics Division  
Argonne National Laboratory  
9700 South Cass Avenue  
Argonne, Illinois 60439  
U.S.A.

## NUCLEAR DATA AND MEASUREMENTS SERIES

The Nuclear Data and Measurements Series presents results of studies in the field of microscopic nuclear data. The primary objective is the dissemination of information in the comprehensive form required for nuclear technology applications. This Series is devoted to: a) Measured microscopic nuclear parameters, b) Experimental techniques and facilities employed in data measurements, c) The analysis, correlation and interpretation of nuclear data, and d) The evaluation of nuclear data. Contributions to this Series are reviewed to assure a high technical excellence and, unless otherwise stated, the contents can be formally referenced. This Series does not supplant formal journal publication but it does provide the more extensive information required for technological applications (e.g. tabulated numerical data) in a timely manner.

## TABLE OF CONTENTS

	<u>Page</u>
ABSTRACT. . . . .	3
I. INTRODUCTION. . . . .	4
II. PHYSICAL PROPERTIES OF AIR. . . . .	5
III. SIMPLE ANALYTIC FORMULATION . . . . .	7
IV. ISOTROPIC SINGLE ELASTIC - SCATTERING FORMULATION . . . . .	10
V. DETAILED SINGLE-SCATTERING FORMULATION. . . . .	15
VI. CONCLUSIONS . . . . .	20
ACKNOWLEDGEMENTS. . . . .	21
APPENDIX I: Listing of FORTRAN IV Code-AIRSC1. . . . .	63
APPENDIX II: Listing of FORTRAN IV Code-AIRSC2. . . . .	69

PROMPT AIR-SCATTERING CORRECTIONS FOR A  
FAST-NEUTRON FISSION DETECTOR:  $E_n \leq 5$  MeV

by

Donald L. Smith

ABSTRACT

Neutrons which have scattered many times in surrounding air and in laboratory objects arrive randomly in time at a detector and can be discriminated by time-of-flight techniques. Neutrons which have scattered only a few times in air reach the detector soon after the primary neutron burst and cannot be distinguished from the latter by time conditions. Most of the prompt air-scattered neutrons have undergone only one elastic collision and it has been shown that the ratio of these singly-scattered to primary neutrons increases linearly with distance from a point source. The energy, time and angular distributions of neutrons which scatter once in surrounding air before reaching a fission detector have been calculated for  $E_n = 0.05 - 5$  MeV using published cross sections. Data corrections for prompt air-scattered neutrons are generally small but not necessarily negligible in high-precision measurements. For example, it has been calculated that this effect leads to a correction of  $\sim 0.2 - 0.3\%$  in a measurement at  $E_n = 1.5$  MeV of the U-238 to U-235 fission cross section ratio if the back-to-back uranium deposits in a double fission detector are situated 10 cm from the neutron source. This correction is significant since  $\sim 1\%$  accuracy is currently sought in fission cross section ratio measurements.

## I. INTRODUCTION

We shall consider a predominantly fast-neutron field whose source is for practical purposes a point (e.g. bombardment of a lithium target with a focused proton beam from an accelerator). The neutron field at an arbitrarily distant observation point is composed of primary neutrons and of neutrons which have scattered in surrounding air and in laboratory objects. The response of a fission detector to these neutrons depends upon the isotopic constituency of the fissionable material in the detector as well as on the characteristics of the field.

Air is a rather sparse medium and the ratio of air-scattered to primary flux is generally small unless the observation point is relatively far from the source. One of the best ways to minimize the influence of air scattering in an experiment is to choose an irradiation position which is as close to the source as possible. Another approach which may be employed to minimize external scattering problems is to irradiate samples and a monitor in the same geometry. External scattering corrections tend to cancel for these relative measurements unless the cross sections involved vary considerably with energy.

Multiple scattering eventually generates a thermal neutron background with weak spatial variation in the vicinity of the source. Thermal neutrons can be extremely troublesome for a fission detector containing a deposit enriched in an isotope with a large thermal fission cross section. Fortunately, time-of-flight techniques can be utilized to reject thermal background in many fast-neutron experiments. Otherwise, it is necessary to place the fission detector close enough to the source so that the thermal correction is manageably small. Hydrogenous laboratory materials such as water, paraffin and concrete are very effective in thermalizing neutrons. Surrounding air and non-hydrogenous laboratory materials also contribute to thermalization. Since experimental techniques exist for minimizing

the effects of thermal neutrons in most fast-neutron experiments, this topic will not be considered further in this paper.

Neutrons which scatter only a few times in air in the vicinity of the source and lose only part of their primary energy can produce fissions and hence cannot be distinguished from primary-neutron fissions by time-of-flight. One could minimize this problem by placing the detector very close to the source, but this is not always feasible. It is the influence of these prompt air-scattered neutrons which has been investigated in the present work. The term "air-scattered neutrons" as used in the remainder of this report implies prompt air-scattered neutrons.

For a monoenergetic point neutron source, define:

$(r, \theta)$  = polar coordinates of the observation point with the source situated at the origin. Air scattering exhibits no azimuthal dependence in a homogeneous medium.

$\Sigma_{T,AIR}$  = macroscopic neutron total cross section for air.

$f_0(\theta)/r^2$  = vacuum flux (neutrons/cm<sup>2</sup> / sec).

$f(r, \theta)/r^2$  = true flux at the observation point (neutrons/cm<sup>2</sup>/sec).

$F(r, \theta)$  = relative intensity of air-scattered and direct neutrons at the observation point.

Then

$$f(r, \theta) = f_0(\theta) [1 + F(r, \theta)] \exp(-r\Sigma_{T,AIR}). \quad (1)$$

Eq. (1) provides no information about the energies, arrival times and angles of incidence for scattered neutrons reaching the detector.

These factors along with properties of the detector determine the relationship between the observed detector response and the neutron field which is to be measured.

## II. PHYSICAL PROPERTIES OF AIR

For the present analysis, dry air is represented by a mixture of nitrogen (79.1%) and oxygen (20.9%) with a total density of 1.205 x

$10^{-3}$  grams per  $\text{cm}^3$  under normal conditions (temperature =  $20^\circ\text{C}$  and pressure = 76 cm Hg) [1]. The only isotopes of nitrogen and oxygen which are significant are N-14 (99.63% of natural nitrogen and O-16 (99.759% of natural oxygen) [2]. The atomic densities of these isotopes are  $4.034 \times 10^{19}$  atoms of N-14 and  $1.066 \times 10^{19}$  atoms of O-16 per  $\text{cm}^3$  of air. The concentrations of the rare gases (argon, etc.) are too small to significantly affect the neutron scattering properties of air. The  $\text{H}_2\text{O}$  vapor content of air is variable, but amounts to  $1.7118 \times 10^{-5}$  grams per  $\text{cm}^3$  of air for  $20^\circ\text{C}$  at the saturation level [1]. This corresponds to  $1.145 \times 10^{18}$  atoms of hydrogen and  $5.724 \times 10^{17}$  atoms of oxygen per  $\text{cm}^3$  of air. The presence of hydrogen in  $\text{H}_2\text{O}$  vapor is likely to have a noticeable effect on the thermalization of neutrons emitted from the source. On the other hand, the  $\text{H}_2\text{O}$  vapor is unlikely to have much influence on the fast-neutron scattering properties of air (except possibly near the oxygen resonance at 0.44 MeV) and therefore,  $\text{H}_2\text{O}$  vapor will be ignored in the present work.

For  $E_n \lesssim 5$  MeV, neutron scattering by N-14 proceeds predominantly via elastic scattering with a small contribution from inelastic scattering through the 3.945 MeV excited state. All scattering from O-16 is elastic for  $E_n < 6.13$  MeV. Total, elastic scattering and inelastic scattering cross sections from an evaluation by J. H. Ray et al. [3] have been used in the present work. Selected cross section values from this reference are listed in Table I (nitrogen) and Table II (oxygen).

Inelastic scattering from nitrogen is assumed to be isotropic in the laboratory. Tables of Legendre coefficients for nitrogen and oxygen elastic scattering angular distributions are given as a function of neutron energy in Ref. 3. These distributions refer to the center-of-mass system and are presented in the form:

$$\left. \frac{d\sigma_E}{d\Omega} \right|_{\text{CM}}(\theta_{\text{CM}}) = (\sigma_E/4\pi) \left[ 1 + \sum_{k=1}^n (2k+1) f_k P_k(\cos\theta_{\text{CM}}) \right] \quad (2)$$

where  $P_k(\cos\theta_{CM})$  is a Legendre polynomial of order  $k$ . The center-of-mass system angular distributions from Ref. 3 were transformed to the laboratory system for use in the present work. Sets of coefficients ( $w_k$ ) were generated where

$$\left. \frac{d\sigma_E}{d\Omega} \right|_{LAB}(\theta_{LAB}) = (\sigma_E/4\pi) \left[ 1 + \sum_{k=1}^m w_k P_k(\cos\theta_{LAB}) \right]. \quad (3)$$

The shapes of the laboratory elastic-scattering angular distributions were reproduced quite well at all energies by using fifth-order expansions ( $m=5$ ). Sets of coefficients  $\{w_k\}$  for various neutron energies are given in Table III (nitrogen) and Table IV (oxygen). Plots of the elastic-scattering angular distributions for selected neutron energies appear in Fig. 1 (nitrogen) and Fig. 2 (oxygen).

### III. SIMPLE ANALYTIC FORMULATION

The analysis in this report assumes a detector which is essentially a parallel-plate ionization chamber with a thin film of fissionable material in the form of a circular disk deposited on one of the plates [4]. Fig. 3 is a schematic diagram which shows the relationship of the fissionable deposit and the point neutron source and defines several geometrical parameters required for calculations. Scattering by other components of the fission chamber constitutes a separate problem which will not be considered here.

It is not hard to derive an expression for the relative intensity of the singly-scattered neutrons to the primary neutrons at the center of the deposit [coordinates (0,0,0) in Fig. 3] if the following approximations are made:

- a. Emission from the source is monoenergetic and isotropic.
- b. Energy loss by neutrons in elastic scattering from nitrogen or oxygen is ignored.
- c. Neutron scattering by nitrogen or oxygen is isotropic in the laboratory.
- d. Flux attenuation along the propagation paths is neglected.

Let

$F_0$  = relative intensity of singly-scattered neutrons to the primary neutrons as computed by the method described in this section.

Then

$$F_0 = (\Sigma_{E,AIR} d^2 / 4\pi) \int_{\text{ALL SPACE}} (1/d_2^2) \delta d_1 \delta \Omega_{S1} \quad (4)$$

where

$\Sigma_{E,AIR}$  = macroscopic neutron elastic scattering cross section for air

and values for  $d_1$  and  $d_2$  as defined in Fig. 3 are computed for  $r_F = 0$  ( $\theta_{S0} = 0$ ).

Azimuthal symmetry and the law of cosines may be applied to obtain the formulas

$$d_2^2 = d^2 + d_1^2 - 2d d_1 \cos \theta_{S1} \quad (5)$$

and

$$F_0 = (\Sigma_{E,AIR} d^2 / 2) \int_0^\infty \delta d_1 \int_0^\pi \delta \Omega_{S1} \sin \theta_{S1} \times (d^2 + d_1^2 - 2d d_1 \cos \theta_{S1})^{-1}. \quad (6)$$

A change of variables and partial integration yields the expression

$$F_0 = (\Sigma_{E,AIR} d / 2) \int_0^\infty \frac{\delta X}{X} \ln \left( \frac{1+X}{1-X} \right). \quad (7)$$

From integral tables in Ref. 1 one obtains

$$\int_0^\infty \frac{\delta X}{X} \ln \left( \frac{1+X}{1-X} \right) = 2 \int_0^1 \frac{\delta X}{X} \ln \left( \frac{1+X}{1-X} \right) = \frac{\pi^2}{2} \quad (8)$$

and consequently

$$F_0 = (\pi^2 \Sigma_{E,AIR} d / 4). \quad (9)$$

The mean free path for elastic scattering  $\lambda_E$  is defined to be the reciprocal of the macroscopic elastic scattering cross section

$\Sigma_{E,AIR}$ , therefore

$$F_0 \approx 2.47 (d/\lambda_E). \quad (10)$$

The interpretation of Eq. (8) is that half of the air-scattered neutrons originate from within a sphere of radius  $d$  centered at the neutron source while the rest of the scattered neutrons come from all space exterior to this sphere. The mean free path for elastic scattering in air can be computed from the formula

$$\lambda_E = [ (4.034 \times 10^{-5}) \sigma_{E,N} + (1.066 \times 10^{-5}) \sigma_{E,O} ]^{-1} \quad (11)$$

using cross section values in barns from Tables I and II (see Section II). Values of  $\lambda_E$  computed from Eq. (11) appear in Table V. The solid curve in Fig. 4 is a plot of  $F_0$  computed with Eq. (10) and values of  $\lambda_E$  from Table V for  $d = 5$  cm. Notice the effect of the oxygen scattering resonance at  $E_n = 0.44$  MeV.

Only singly-scattered neutrons were considered in the preceding analysis. A rudimentary argument for neglecting higher-order scattering will now be presented. Let us assume that time-of-flight conditions preclude detection of any neutron which has propagated along a path (not necessarily in a straight line) of length exceeding  $L$ . By definition of the mean free path  $\lambda_E$ , the average number of collisions experienced by a neutron along a path of length  $L$  is  $L/\lambda_E$ . The probability of the neutron experiencing exactly  $N$  collisions is given by the Poisson distribution

$$P_N = \frac{(L/\lambda_E)^N e^{-L/\lambda_E}}{N!} \quad (12)$$

From Eq. (12) it is seen that the probability of zero collisions  $P_0$  is  $e^{-L/\lambda_E}$  which is exactly what one would expect since  $e^{-L/\lambda_E}$  is the attenuation coefficient. The probability of experiencing any sort of collision (without specifying the order) is just  $(1 - e^{-L/\lambda_E})$ . The probability  $P_1$  of a single collision is  $(L/\lambda_E) e^{-L/\lambda_E}$  and, in general, the ratio of  $P_N$  to  $P_{N-1}$  is simply  $(L/N\lambda_E)$ . From Table V it is seen that  $\lambda_E = 6854$  cm for  $E_n = 1$  MeV. On the other hand, a reasonable time limitation imposed by time-of-flight discrimination would be  $\sim 20$  nanoseconds. This implies  $L = 277$  cm and a corresponding ratio of  $P_2$  to  $P_1$  of  $\sim 0.02$ . Higher orders of scattering are

even more negligible.

Langsdorf has shown by means of an analysis resembling that which led to Eq. (9) that the ratio of doubly air-scattered neutrons to primary neutrons can be approximated by a relatively simple formula for small values of  $d/\lambda_E$  [5]. Application of this formula for  $E_n = 1$  MeV and  $d = 5$  cm yields a ratio of  $\sim 10^{-5}$  for doubly scattered to primary neutrons and  $\sim 0.006$  for the ratio of doubly scattered to singly scattered neutrons. This result indicates that the rudimentary approach discussed in the preceding paragraph may overestimate the importance of higher-order scattering. Consequently, only single scattering will be considered for the remainder of this report.

#### IV. ISOTROPIC SINGLE ELASTIC-SCATTERING FORMULATION

The relative intensity of scattered and primary neutrons can be estimated easily from Eqs. (10) and (11). The only additional piece of information which the formulation in Section III provides is that half of the air-scattered flux originates from within a distance  $d$  of the source. A different approach is required to study the effects of finite detector size and to determine the incidence-angle and arrival-time distributions for air-scattered neutrons. These additional aspects will be investigated in the present section within the framework of the approximations stated in Section III.

The appropriate geometry for the following analysis is shown in Fig. 3. It is advantageous to define a set of cylindrical coordinates  $(r_A, \phi_A, Z_A)$  with origin  $(0,0,0)$  at the center of the uranium deposit. The point neutron source is situated on the axis at coordinates  $(0,0,d)$ . The uranium deposit is taken to be a very thin circular disk with radius  $R_{\text{DISK}}$ . Let

$F_1$  = relative number of air-scattered neutrons to primary neutrons incident upon the deposit as computed by the method described in this section.

then

$$F_1 = (\Sigma_{E,AIR}/4\pi) \frac{\left[ \int_0^{R_{DISK}} \delta r_F \int_0^\infty \delta r_A \int_{-\infty}^\infty \delta z_A \int_0^{2\pi} \delta \phi_A \Psi(d, r_F, r_A, z_A, \phi_A) \right]}{\left[ \int_0^{R_{DISK}} \delta r_F \Phi(d, r_F) \right]} \quad (13)$$

where

$$\Phi(d, r_F) = r_F / (r_F^2 + d^2) \quad (14)$$

$$\Psi(d, r_F, r_A, z_A, \phi_A) = (r_A r_F / d_1^2 d_2^2) \quad (15)$$

$$d_1^2 = X_A^2 + Y_A^2 + (z_A - d)^2 \quad (16)$$

$$d_2^2 = (X_A - r_F)^2 + Y_A^2 + z_A^2 \quad (17)$$

The indicated integration of Eq. (13) extends over the surface of the disk and over all air space. Since most of the air-scattered neutrons come from the vicinity of the source, it is reasonable to set limits on the region of air space included in the evaluation of  $F_1$ . Thus

$$F_1 \approx (\Sigma_{E,AIR}/4\pi) \frac{\left[ \int_0^{R_{DISK}} \delta r_F \int_0^{R_{A,MAX}} \delta r_A \int_{-Z_{A,MAX}}^{+Z_{A,MAX}} \delta \phi_A \Psi(d, r_F, z_A, \phi_A) \right]}{\left[ \int_0^{R_{DISK}} \delta r_F \Phi(d, r_F) \right]} \quad (18)$$

where  $R_{A,MAX}$  and  $Z_{A,MAX}$  are limits on the coordinates  $r_A$  and  $z_A$  which define a pillbox surrounding the uranium deposit. The integrals appearing in Eq. (18) are evaluated by a Monte-Carlo technique. The expression

$$F_1 \approx \Sigma_{E,AIR} \frac{\left[ \sum_{j=1}^{N_{HIST}} \Psi_j \right] / N_{HIST}}{\left[ \sum_{j=1}^{M_{HIST}} \Phi_j \right] / M_{HIST}} \quad (19)$$

is an approximation to Eq. (18) which improves in accuracy with increased numbers  $N_{HIST}$  and  $M_{HIST}$  of sampling histories. ( $M_{HIST}$  can

be considerably smaller than  $N_{\text{HIST}}$ ). Choice of values for  $M_{\text{HIST}}$  and  $N_{\text{HIST}}$  is a matter of compromise between computational time and statistical stability. Random values for  $r_F$ ,  $r_A$ ,  $Z_A$  and  $\phi_A$  were computed for each history from the equations

$$r_F = R_{\text{DISK}} \eta_F \quad (0 < \eta_F \leq 1) \quad (20)$$

$$r_F = R_{A,\text{MAX}} \eta_R \quad (0 < \eta_R \leq 1) \quad (21)$$

$$Z_A = -Z_{A,\text{MAX}} + 2Z_{A,\text{MAX}}\eta_Z \quad (22)$$

$$(0 < \eta_Z \leq 1)$$

$$\phi_A = 2\pi\eta_\phi \quad (0 < \eta_\phi \leq 1) \quad (23)$$

where  $\eta_F$ ,  $\eta_R$ ,  $\eta_Z$  and  $\eta_\phi$  are random numbers.

An advantage of this method is that it permits one to easily calculate distributions and history averages of other parameters using the same weighting factors  $\mathfrak{F}_j$  and  $\mathfrak{G}_j$  from Eqs. (14) and (15). The arrival-time distribution for air-scattered neutrons is of interest for time-of-flight applications because one wishes to know to what extent the air-scattered neutrons straggle with respect to the primary neutrons and thereby produce a "late-arrival" tail on the time peak generated by a pulsed neutron source. The minimum flight time from the neutron source to the uranium disk is given by

$$T_{\text{MIN}} = d/v_n \quad (24)$$

where

$$v_n = \text{velocity of the neutrons}$$

and this corresponds to propagation along the axis. The longest flight time for primary neutrons is given by

$$T_{\text{MAX}} = (d^2 + R_{\text{DISK}}^2)^{1/2}/v_n \quad (25)$$

and  $(T_{\text{MAX}} - T_{\text{MIN}})$  is usually smaller than the experimental time resolution. The flight time for an air-scattered neutron (with no energy loss) is given by

$$T = (d_1 + d_2)/v_n \quad (26)$$

which could be significant if  $(d_1 + d_2) \gg d$ . During the process of evaluating the numerator of Eq. (19) one can compute flight times  $T_j$ , each weighted by the appropriate value  $\mathcal{W}_j$ , and thereby generate a time distribution. In the present work, the time interval  $(0, T_{\text{RANG}})$  was divided into  $N_{\text{TIME}}$  equal time intervals. If the following inequality

$$[(k-1)T_{\text{RANG}}/N_{\text{TIME}}] \leq (T_j - T_{\text{MIN}}) \leq [k T_{\text{RANG}}/N_{\text{TIME}}] \quad (27)$$

is satisfied for the  $j$ th history, then  $\mathcal{W}_j$  is added to the weight factor  $\mathcal{J}_k$  for the  $k$ th "bin" of the discrete time distribution function. The collection of values  $\{\mathcal{J}_k\}$  obtained from following  $N_{\text{HIST}}$  histories defines the unnormalized time distribution function. Contributions from histories for which  $(T_j - T_{\text{MIN}})$  exceed  $T_{\text{RANG}}$  are recorded in an "overflow" bin. Use of such an "overflow" bin permits one to calculate how many events will be lost as a result of air scattering when a "window" is placed on the time peak during a measurement.

The angle of incidence  $\theta_I$  for neutrons which scatter from air in the vicinity of the point  $(X_A, Y_A, Z_A)$  and subsequently reach the uranium deposit at the point  $(r_F, 0, 0)$  can be calculated by analytic geometry (see Fig. 3). The angle-of-incidence distribution function and the history average  $\bar{\theta}_I$  can be computed in a manner similar to that used for obtaining the arrival-time distribution function. The angle-of-incidence distribution function is a useful aid in understanding the air-scattering problem because it indicates the direction from which most of the air-scattered neutrons impinge on the uranium deposit.

Calculations were made on a digital computer using the formalism described in the preceding paragraphs. See Appendix I for a listing of the FORTRAN IV code AIRSC1 which was written to perform these calculations. The values  $M_{\text{HIST}} = 2000$  and  $N_{\text{HIST}} = 20000$  were found to yield sufficient statistical stability for the present work. Values of  $F_1$  computed from Eq. (13) should approximate corresponding values of  $F_0$  from Eq. (10)--if finite uranium deposit size effects are neglected--since both formulations of the problem are based on

the same set of physical assumptions. To test this point and to determine how large  $R_{A,MAX}$  and  $Z_{A,MAX}$  have to be so that Eq. (18) becomes a good approximation to Eq. (13) the following two sets of calculations were made:

- a. The ratio  $F_1/F_0$  was computed for several values of  $R_{A,MAX}$  ( $= Z_{A,MAX}$ ) with  $E_n = 1$  MeV,  $R_{DISK} = 1.27$  cm and  $d = 5$  cm.
- b. The ratio  $F_1/F_0$  was computed for several values of  $d$  with  $E_n = 1$  MeV,  $R_{DISK} = 1.27$  cm and  $R_{A,MAX} = Z_{A,MAX} \geq 10 d$ .

The results of these sets of calculations appear in Figs. 5 - 8. From the values of  $F_1/F_0$  plotted in Fig. 5 one can conclude that about half of the air-scattered flux originates from the region of air space for which  $R_{A,MAX} = Z_{A,MAX} \leq d$  which is in agreement with the interpretation of Eq. (8). From Fig. 6 it is evident that the effects of the finite size of the uranium deposit essentially disappear for  $d/R_{DISK} > 3$ . This fact can also be deduced from Fig. 7 which is a plot of  $\bar{\theta}_I$  vs.  $d/R_{DISK}$ .  $\bar{\theta}_I$  approaches a limit of  $\sim 60^\circ$  for  $d/R_{DISK} > 3$ . The variation in shape of the angle-of-incidence distribution functions with  $d/R_{DISK}$  is shown in Fig. 8. The effect of finite uranium deposit size is to produce a forward-angle dip in the distribution function. This structural feature is still evident for  $d/R_{DISK} \sim 5$ . However, for larger values of  $d/R_{DISK}$  this feature disappears and the distribution function becomes approximately linear in  $\bar{\theta}_I$ .

Another set of calculations was made for various neutron energies with  $R_{DISK} = 1.27$  cm,  $d = 5$  cm ( $d/R_{DISK} = 3.94$ ) and  $R_{A,MAX} = Z_{A,MAX} > 10 d$ . The resulting values of  $F_1$  are plotted in Fig. 4. Except for some statistical fluctuation, the values of  $F_0$  and  $F_1$  are in excellent agreement. Corresponding scattered neutron arrival-time distributions were obtained from the same set of calculations and these appear in Fig. 9. Notice that even for low energies most of the scattered neutrons arrive at the uranium deposit within a few nanoseconds after the primary neutrons. It is clear that it is not feasible to eliminate the effects of prompt air-scattered neutrons by setting a "window" on the direct-neutron time peak.

## V. DETAILED SINGLE-SCATTERING FORMULATION

Several approximations found in Section III and IV can be relaxed in order to provide a more general treatment of air scattering. Those features of the problem which will be taken into consideration in the present section are:

- The angular distribution and variation of energy with emission angle for neutrons from the source.
- Attenuation of both primary and air-scattered neutrons by intervening air.
- Energy loss by neutrons in elastic and inelastic scattering from nitrogen and oxygen.
- Angular distribution effects in elastic scattering from nitrogen and oxygen.
- Finite thickness of the uranium deposit in the fission chamber.
- Variations in the isotopic content of the fission deposit and energy dependence of the fission cross section.

The quantity  $F_2$  is defined as:

$F_2$  = relative number of fissions produced in the fission detector by air-scattered and primary neutrons.

Monte-Carlo methods similar to those used for calculation of  $F_1$  in Section IV have been applied in calculation of  $F_2$ . The parameters  $r_A$ ,  $\phi_A$ ,  $Z_A$  and  $r_F$  were selected at random and computation was limited to the region of space defined by  $R_{A,MAX}$  and  $Z_{A,MAX}$  as described in Section IV. Thus

$$F_2 \approx 2\pi R_{A,MAX} Z_{A,MAX} \frac{\left[ \left( \sum_{j=1}^{N_{HIST}} \right) / N_{HIST} \right]}{\left[ \left( \sum_{j=1}^{M_{HIST}} \right) / M_{HIST} \right]} \quad (28)$$

where for each  $j$ ,

$$\mathcal{Q} = f_{SO} \cos\theta_{SO} \left( \frac{r_f}{d_0^2} \right) \exp(-d_0 \Sigma_{T,AIR,0}) \quad (29)$$

$$X \left( \frac{\Sigma_{F,U,0}}{\Sigma_{T,U,0}} \right) \left[ 1 - \exp(-\tau \Sigma_{T,U,0} / \cos \theta_{SO}) \right]$$

and

$$\begin{aligned} \phi &= f_{S1} \cos \theta_I \left( \frac{r_A r_F}{d_1^2 d_2^2} \right) \exp(-d_1 \Sigma_{T,AIR,1}) X \\ &X \left\{ \sum_{k=1}^3 \left( \frac{\delta \Sigma}{\delta \Omega} \text{AIR}, 1k \right) \exp(-d_2 \Sigma_{T,AIR,2}) X \right. \\ &\left. X \left( \frac{\Sigma_{F,U,2k}}{\Sigma_{T,U,2k}} \right) \left[ 1 - \exp(-\tau \Sigma_{T,U,2k} / \cos \theta_I) \right] \right\} \end{aligned} \quad (30)$$

with

$f_{SO}$  = neutron source strength as a function of angle

$\theta_{SO}$  = neutron emission angle.

$\left( \frac{\delta \Sigma}{\delta \Omega} \text{AIR}, 1k \right)$  = normalized macroscopic differential cross section for the k-th scattering process for air.

$\tau$  = uranium deposit thickness.

The subscript "T" designates a total cross section. The subscript "F" designates a fission cross section. The subscripts "0", "1" and "2" designate the neutron paths with respective lengths  $d_0$ ,  $d_1$  and  $d_2$  as shown in Fig. 3. The subscript "U" designates a process involving the uranium deposit. Finally the subscript "k" designates a particular neutron scattering process in air (k = 1: nitrogen elastic scattering, k = 2: nitrogen inelastic scattering, and k = 3: oxygen elastic scattering). All cross sections designated by a " $\Sigma$ " are macroscopic.

A digital computer was utilized for calculations of  $F_2$ . A listing of the FORTRAN IV code AIRSC2 employed in the calculations

appears in Appendix II. Changes in neutron energy following a scattering process (e.g. Ref. 6) can be calculated with AIRSC2. Thus it was possible to determine a distribution of fission events vs. incident neutron energy. This distribution function is quite useful since it enables one to deduce an average energy for scattered neutrons incident on the uranium deposit.

Calculations were made for U-235 enriched deposits and also for deposits which were enriched in U-238. See Table VI for the deposit compositions used in most of the calculations. The deposits were assumed to be uniformly thick. Fission cross sections required for this work were obtained from the ENDF/B-III set [7], from compilations by W. G. Davey [8,9] and from measurements by Meadows [10] (see Table VII for values of these cross sections).

The first set of calculations was carried out with the intent of comparing predictions from the detailed single-scattering formulation with those from Sections III and IV for several neutron energies and a fixed geometry. The parameters used for these calculations are indicated in Table VIII. Unless otherwise stated, the parameters for all other sets of calculations discussed in this section are those from Table VIII. Integrations were carried out over a finite air volume ( $R_{A,MAX} = Z_{A,MAX} = 30$  cm). Resultant  $F_2$  values were corrected for excluded space by means of data from Fig. 5. Fig. 10 is a plot of  $F_0$  and  $F_2$  for both a U-235 enriched and a U-238 enriched deposit (see Table VI) vs. source neutron energy. The agreement of  $F_2$  and  $F_0$  [computed from Eqs. (10) and (11)] is reasonably good at most energies for the U-235 monitor. The agreement is poor over the energy range 0.85 - 2 MeV for the U-238 monitor. The explanation for this result is that the U-238 fission cross section increases sharply at  $E_n \approx 1$  MeV and those neutrons which are scattered by air generally lose sufficient energy so that they contribute far fewer fissions per neutron than the primary neutrons. At higher energies, the neutron energies after scattering remain above this threshold region. Figs. 11 and 12 are plots of the number of fissions vs. the energy of incidence of scattered neutrons at a U-235 enriched and U-238 enriched

deposit respectively. The effect of air scattering on the neutron energy spectra is evident. Spectral plots for 5 MeV primary energy show the effect of inelastic scattering from nitrogen. The inelastically scattered neutrons have very little effect on a U-238 deposit below  $\sim 5$  MeV because the U-238 fission cross section is small for the low-energy inelastically scattered neutrons.

Next, the influence of uranium deposit thickness on the calculation of  $F_2$  was investigated. Calculations were made only for U-235 enriched deposits. Deposits with thicknesses ranging from 0.001 to 1000 times that for the deposit described in Table VI were considered. Otherwise, the parameters employed were those indicated in Table VIII. A primary energy of 1 MeV was assumed for this set of calculation. The results appear in Table IX. Clearly,  $F_2$  is insensitive to the deposit thickness for all realistic deposits.

The detailed formulation is capable of taking the neutron source distribution into consideration, so this aspect was investigated next. In order to make a systematic investigation, hypothetical neutron source distributions of the form

$$S(\theta_{\text{LAB}}) = 1 + w_1 P_1 (\cos \theta_{\text{LAB}}) \quad (31)$$

were assumed and  $w_1$  was varied from  $w_1 = -1$  (strong backward peaking) through  $w_1 = 0$  (isotropic) to  $w_1 = 1$  (strong forward peaking). The calculations were made assuming a monoenergetic neutron source of 1 MeV. Otherwise, the parameters of the calculation were as indicated in Table VIII. Resulting values of  $F_2$  are plotted in Fig. 13. The conclusion from this analysis is that the ratio of fissions from air-scattered neutrons and primary neutrons is only moderately sensitive to the neutron source distribution provided that the distribution is more or less forward peaked ( $0 < w_1 \lesssim 1$ ). However, the relative contribution from air-scattered neutrons increases sharply if the source distribution is more or less backward peaked ( $-1 \lesssim w_1 < 0$ ). In the latter case, the approximate treatments of Sections III and IV do not give reasonable values for the air scattering correction. In practice, most neutron source reactions tend to emit neutrons pre-

dominantly at forward laboratory angles.

The preceding calculations assumed monoenergetic neutrons from the source. In practice, neutron energy varies with emission angle because of the kinematics of source reactions involving finite nuclei. In order to investigate the effect of neutron source kinematic broadening, calculations were performed assuming hypothetical two-body neutron producing reactions with  $Q = 0$  initiated by a projectile with mass equal to a neutron ( $A_1 = 1.009$  amu). Target nuclei with masses (in amu)  $A_2 = 2, 5, 10, 20, 50, 100$  and infinity were considered. The neutron source distributions were assumed to be isotropic. Other parameters of the calculation were as indicated in Table VIII. Calculations were made with primary projectile energies  $E_1 = 1$  MeV and 3 MeV for both U-235 and U-238 enriched deposits. The results of these calculations appear in Table X. The conclusion to be drawn from these results is that  $F_2$  is only moderately sensitive to target mass  $A_2$  for a U-235 enriched deposit. The sensitivity is somewhat greater for a U-238 enriched monitor, presumably because of the more pronounced energy dependency of the fission cross section for U-238.

The influence of the nitrogen and oxygen elastic scattering angular distributions cannot be very large because the agreement of  $F_0$  from Section III and  $F_2$  calculated for similar geometry and neutron source characteristics is fairly good except for a U-238 enriched deposit when  $E_n = 0.85 - 2$  MeV. In order to check this point further, calculations were made for several primary energies with the nitrogen scattering assumed to be isotropic and then with the oxygen scattering assumed isotropic. All other parameters were as indicated in Table VIII. The results of this analysis appear in Table XI. As expected, the substitution of isotropy for either nitrogen or oxygen elastic scattering has a relatively moderate effect on  $F_2$ .

A final application of the detailed single scattering formulation was to calculate  $F_2$  for a realistic neutron source reaction. Angular distributions for the  ${}^7\text{Li}(p,n){}^7\text{Be}$  reaction, which produces

two distinct groups having Q-values of -1.644 and -2.079 MeV respectively, have been measured for several proton energies by S. A. Elbaker et al. [11]. Coefficients for these distributions, expressed in the laboratory system, are given in Table XII for reference. The results of calculations for a U-235 deposit appear in Fig. 14. Except for the neutron source specifications, the parameters indicated in Table VIII were used in these calculations. Fig. 15 shows the results from a similar set of calculations for a U-238 enriched deposit. Generally, the values of  $F_2$  are smaller for the  ${}^7\text{Li}(p,n){}^7\text{Be}$  neutron groups than for an isotropic, mono-energetic source. An exception is the set of  $F_2$  values for a U-235 deposit and the  $Q = 2.079$  MeV group from the  ${}^7\text{Li}(p,n){}^7\text{Be}$  reaction.

## VI. CONCLUSIONS

The number of air scattered neutrons incident upon a fission chamber is small relative to the direct flux for most experimental configurations. The relative importance of air-scattered neutrons is dominated by the distance  $d$  from the source to the fission deposit and by the mean free path  $\lambda_E$  for elastic scattering. These two parameters enter as the ratio  $(d/\lambda_E)$ . The effect of air scattering generally decreases with increased neutron energy; however, there is a sharp increase in the vicinity of the 0.44 MeV oxygen resonance. Since most of the air scattering occurs near to the source, it is not possible to discriminate against the air-scattered neutrons by means of time of flight. Kinematic broadening of source neutron energies and the shapes of nitrogen and oxygen elastic scattering angular distributions have only a moderate effect on air scattering. The relative importance of air scattering is very sensitive to the angular distribution of the source neutrons and is observed to increase sharply if the source peaks toward back angles. The effect of air scattering on a U-238 enriched deposit is smaller than that for a U-235 deposit for neutrons in the vicinity of 0.82 - 2 MeV where the U-238 fission cross section increases rapidly with energy. The ex-

planation for this effect is that air scattering degrades the neutron energies into a region where the U-238 fission cross section is small. This phenomenon could introduce a noticeable error in measurement of the ratio of the U-238 to U-235 fission cross sections. For example, consider a hypothetical measurement made with a double fission chamber containing two uranium deposits (one enriched in U-235 and the second enriched in U-238) on adjacent backing plates 10 cm from an isotropic fast-neutron source. From Fig. 10 we can deduce that the air-scattering correction is  $\sim 0.3\%$  for U-235 and  $\sim 0.06\%$  for U-238 at  $E_n = 1.5$  MeV. Consequently, there is a net correction of  $\sim 0.24\%$  in the cross section ratio. This is not a negligible correction since experimenters are currently striving for accuracies of  $\sim 1\%$  in fission cross section ratio measurements.

#### ACKNOWLEDGEMENTS

The author is indebted to J. W. Meadows, P. T. Guenther and A. B. Smith for valuable suggestions which they made during the course of this work.

## REFERENCES

1. Handbook of Chemistry and Physics, 41st Edition, ed. C. D. Hodgman, Chemical Rubber Publishing Company, Cleveland, Ohio, U.S.A. (1959).
2. C. A. Rohrman, "Chart of the Nuclides", compiled at Battelle-Northwest, Richland, Washington 99352, U.S.A., for the U.S. Atomic Energy Commission (1969).
3. J. H. Ray, G. Grochowski and E. S. Troubetzkoy, "Neutron Cross Sections of Nitrogen, Oxygen, Aluminum, Silicon, Iron, Deuterium and Beryllium", Report No. UNC-5139, United Nuclear Corporation, Elmsford, New York 10523 (1965).
4. R. W. Lamphere, "Fission Detectors", in Fast Neutron Physics I eds. J. B. Marion and J. L. Fowler, Interscience, New York, 449 (1960).
5. A. Langsdorf, Jr., "Neutron Collimation and Shielding for Experimental Purposes", in Fast Neutron Physics I, eds. J. B. Marion and J. L. Fowler, Interscience, New York, 721 (1960).
6. A. S. Langsdorf, J. E. Monahan and W. A. Reardon, "A Tabulation of Neutron Energies from Monoenergetic Protons on Lithium", Report No. ANL-5219, Argonne National Laboratory, Argonne, Illinois 60439 (1954).
7. National Neutron Cross Section Center, Brookhaven National Laboratory, Upton, New York 11973, U.S.A.
8. W. G. Davey, "Selected Fission Cross Sections for  $^{232}\text{U}$ ,  $^{233}\text{U}$ ,  $^{234}\text{U}$ ,  $^{235}\text{U}$ ,  $^{236}\text{U}$ ,  $^{237}\text{Np}$ ,  $^{238}\text{U}$ ,  $^{239}\text{Pu}$ ,  $^{241}\text{Pu}$  and  $^{242}\text{Pu}$ ", Nuclear Science and Engineering 32, 35 (1969).
9. W. G. Davey, "An Analysis of the Fission Cross Sections of  $^{232}\text{Th}$ ,  $^{233}\text{U}$ ,  $^{234}\text{U}$ ,  $^{235}\text{U}$ ,  $^{236}\text{U}$ ,  $^{237}\text{Np}$ ,  $^{238}\text{U}$ ,  $^{239}\text{Pu}$ ,  $^{241}\text{Pu}$  and  $^{242}\text{Pu}$  from 1 keV to 10 MeV", Nuclear Science and Engineering 26, 149 (1966).
10. J. W. Meadows, "The Ratio of the Uranium-238 to Uranium-235 Fission Cross Sections from 1 to 5 MeV", Nuclear Science and Engineering 49, 310 (1972).
11. S. A. Elbaker, I. J. Van Heerden, W. J. McDonald and G. C. Neilson, "Measurements of Neutron Angular Distributions from the  $^7\text{Li}(p,n)^7\text{Be}$  Reaction", Nuclear Instruments and Methods 105, 519 (1972).

TABLE I

Selected Cross Section Values for N-14<sup>a</sup>Total Cross Sections

$E_n$ (MeV)	$\sigma_{T,N}$ (barns)	$E_n$ (MeV)	$\sigma_{T,N}$ (barns)	$E_n$ (MeV)	$\sigma_{T,N}$ (barns)
0.0 <sup>b</sup>	10.5	1.096	2.48	2.438	1.51
0.01	7.8	1.152	1.73	2.833	1.48
0.403	3.29	1.211	1.61	2.978	1.66
0.424	5.01	1.273	1.86	3.131	1.67
0.455	3.35	1.338	2.83	3.292	1.73
0.468	2.59	1.479	2.07	3.638	1.75
0.601	1.8	1.555	2.37	3.824	1.69
0.632	1.91	1.635	2.4	4.226	1.71
0.665	2.38	1.718	2.05	4.443	1.78
0.7	2.29	1.806	2.46	4.671	1.86
0.734	2.06	1.899	1.85	4.91	1.37
0.943	1.26	2.099	1.58	5.162	1.63
0.991	1.55	2.206	1.66		
1.042	2.21	2.32	1.56		

TABLE I (Contd.)

Elastic Scattering Cross Sections

$E_n$ (MeV)	$\sigma_{E,N}$ (barns)	$E_n$ (MeV)	$\sigma_{E,N}$ (barns)	$E_n$ (MeV)	$\sigma_{E,N}$ (barns)
0.0 <sup>b</sup>	10.5	1.152	1.72	3.131	1.36
0.01	7.8	1.211	1.596	3.292	1.36
0.403	3.29	1.273	1.84	3.46	1.34
0.424	5.01	1.338	2.73	3.638	1.37
0.455	3.35	1.479	1.95	3.824	1.33
0.468	2.59	1.555	2.32	4.02	1.24
0.601	1.8	1.635	2.35	4.226	1.23
0.632	1.76	1.718	2.0	4.443	1.35
0.665	2.21	1.806	2.3	4.671	1.46
0.699	2.23	1.899	1.77	4.91	1.05
0.734	2.03	2.695	1.25	5.16	1.32
0.943	1.25	2.833	1.24		
1.096	2.48	2.978	1.39		

Inelastic Scattering Cross Sections (Q=-3.945 MeV)

$E_n$ (MeV)	$\sigma_{I,N}$ (barns)	$E_n$ (MeV)	$\sigma_{I,N}$ (barns)	$E_n$ (MeV)	$\sigma_{I,N}$ (barns)
0.0 <sup>b</sup>	0.0	4.226	$6.763 \times 10^{-3}$	5.0	$1.0 \times 10^{-2}$
3.945	0.0	4.443	$7.73 \times 10^{-3}$		
4.02	$1.751 \times 10^{-3}$	4.671	$8.583 \times 10^{-3}$		

TABLE I(Contd.)

- a. Values taken from Ref. 3.
- b. A "zero-energy" cross section value is included in the tables to provide a lower limit for interpolation.

TABLE II

Selected Cross Section Values for 0-16<sup>a</sup>Total Cross Sections

$E_n$ (MeV)	$\sigma_{T,0}$ (barns)	$E_n$ (MeV)	$\sigma_{T,0}$ (barns)	$E_n$ (MeV)	$\sigma_{T,0}$ (barns)
0.0 <sup>b</sup>	3.7	1.152	3.03	2.563	1.23
0.284	3.71	1.211	3.01	2.695	1.22
0.383	4.26	1.273	4.55	2.833	1.28
0.403	6.04	1.338	3.8	3.131	1.8
0.424	11.2	1.479	2.28	3.292	2.86
0.445	14.5	1.555	2.28	3.46	3.02
0.468	9.5	1.635	3.47	4.02	1.7
0.492	5.71	1.718	3.02	4.226	1.82
0.518	4.28	1.899	2.72	4.443	1.88
0.544	3.64	2.099	1.4	4.671	1.11
0.853	3.03	2.32	0.779	4.91	1.13
0.991	7.47	2.438	0.919	5.162	1.6

TABLE II (Contd.)

Elastic Scattering Cross Sections

$E_n$ (MeV)	$\sigma_{E,0}$ (barns)	$E_n$ (MeV)	$\sigma_{E,0}$ (barns)	$E_n$ (MeV)	$\sigma_{E,0}$ (barns)
0.0 <sup>b</sup>	3.7	1.211	3.01	2.695	1.22
0.383	4.26	1.273	4.55	2.833	1.28
0.403	6.04	1.338	3.8	3.131	1.8
0.424	11.2	1.479	2.28	3.292	2.86
0.445	14.5	1.555	2.28	3.46	3.02
0.468	9.5	1.635	3.47	3.638	2.98
0.492	5.71	1.718	3.02	3.82	2.89
0.518	4.28	1.899	2.72	4.02	1.63
0.544	3.64	2.099	1.4	4.443	1.84
0.853	3.03	2.32	0.779	4.671	1.06
0.991	7.47	2.438	0.919	4.91	1.03
1.152	3.03	2.563	1.23	5.162	1.54

a. Values taken from Ref. 3.

b. A "zero-energy" cross section value is included in the table to provide a lower limit for interpolation.

TABLE III

Legendre Coefficients for Nitrogen Laboratory  
Elastic-Scattering Angular Distributions<sup>a</sup>

<u>w<sub>1</sub></u>					
$E_n$ (MeV)	$w_1$	$E_n$ (MeV)	$w_1$	$E_n$ (MeV)	$w_1$
0.0 <sup>b</sup>	0.14	1.4	0.58	3.0	0.2
1.0	0.305	1.48	0.48	3.4	0.2
1.02	0.19	1.62	0.75	4.25	0.8
1.15	0.66	1.8	0.25	4.95	0.5
1.3	0.3	2.25	0.74	5.4	0.51
<u>w<sub>2</sub></u>					
$E_n$ (MeV)	$w_2$	$E_n$ (MeV)	$w_2$	$E_n$ (MeV)	$w_2$
0.0 <sup>b</sup>	0.0	1.45	0.14	3.12	1.56
1.0	0.0	1.8	0.69	3.45	1.78
1.15	0.45	2.1	0.24	3.92	1.91
1.25	0.21	2.45	0.65	4.25	1.83
1.35	0.375	2.8	1.24	5.15	0.96

TABLE III (Contd.)

w<sub>3</sub>

$E_n$ (MeV)	$w_3$	$E_n$ (MeV)	$w_3$	$E_n$ (MeV)	$w_3$
0.0 <sup>b</sup>	0.0	1.65	0.2	2.7	2.7
1.0	0.0	1.7	0.11	3.3	0.35
1.2	0.21	2.1	0.12	4.25	0.57
1.35	0.13	2.35	0.35	5.15	0.65

w<sub>4</sub>

$E_n$ (MeV)	$w_4$	$E_n$ (MeV)	$w_4$	$E_n$ (MeV)	$w_4$
0.0 <sup>b</sup>	0.0	3.46	0.641	4.671	0.743
2.9	0.0	3.824	0.549	4.91	0.854
2.978	0.074	4.02	0.458	5.162	0.731
3.131	0.32	4.23	0.453		
3.292	0.499	4.443	0.546		

TABLE III (Contd.)

<u>w<sub>5</sub></u>					
$E_n$ (MeV)	$w_5$	$E_n$ (MeV)	$w_5$	$E_n$ (MeV)	$w_5$
0.0 <sup>b</sup>	0.0	4.443	0.136	4.91	0.498
4.4	0.0	4.671	0.303	5.162	0.534

- a. Legendre coefficients are derived from data in Ref. 3. Angular distributions may be calculated from Eq. (3), however the coefficients listed above or interpolated values may not yield proper normalization. The computed distributions should be renormalized prior to use in scattering calculations.
- b. A "zero-energy" coefficient value is included in the table to provide a lower limit for interpolation.

TABLE IV

Legendre Coefficients for Oxygen Laboratory  
Elastic-Scattering Angular Distributions<sup>a</sup>

<u><math>w_1</math></u>					
$E_n$ (MeV)	$w_1$	$E_n$ (MeV)	$w_1$	$E_n$ (MeV)	$w_1$
0.0 <sup>b</sup>	0.12	1.33	1.02	3.64	1.16
0.15	0.06	1.5	0.24	3.83	1.0
0.36	-0.59	1.7	0.0	4.05	1.01
0.46	1.32	2.05	0.42	4.25	0.77
0.8	0.3	2.5	0.08	4.45	1.39
1.0	0.22	2.95	0.34	4.85	0.4
1.05	-0.06	3.13	0.73	5.17	0.38
1.2	-0.18	3.3	0.56		

<u><math>w_2</math></u>					
$E_n$ (MeV)	$w_2$	$E_n$ (MeV)	$w_2$	$E_n$ (MeV)	$w_2$
0.0 <sup>b</sup>	0.0	1.02	1.65	3.3	1.58
0.1	0.0	1.5	0.24	4.05	0.82
0.35	-0.26	1.65	0.48	4.45	1.46
0.43	0.81	1.7	0.18	4.67	0.3
0.58	0.08	2.1	0.64	5.15	0.98
0.82	-0.16	2.45	-0.02		
0.9	-0.06	3.0	0.26		

TABLE IV (Contd.)

<u><math>w_3</math></u>					
$E_n$ (MeV)	$w_3$	$E_n$ (MeV)	$w_3$	$E_n$ (MeV)	$w_3$
0.0 <sup>b</sup>	0.02	1.55	0.3	3.62	0.94
0.25	-0.095	1.64	0.62	3.85	0.94
0.4	0.24	1.75	0.3	4.15	0.6
0.65	-0.02	2.0	0.075	4.45	1.46
0.85	-0.04	2.7	0.02	4.7	0.82
0.98	0.38	3.0	0.18	5.15	1.22
1.15	-0.1	3.2	0.86		
1.4	0.48	3.45	0.6		

<u><math>w_4</math></u>					
$E_n$ (MeV)	$w_4$	$E_n$ (MeV)	$w_4$	$E_n$ (MeV)	$w_4$
0.0	0.0	1.1	-0.02	3.3	0.01
0.2	0.18	1.25	0.26	3.62	0.33
0.32	-0.08	1.4	0.12	4.1	0.04
0.43	0.14	1.52	0.8	4.5	0.56
0.52	-0.07	1.73	0.32	4.7	0.46
0.6	0.064	2.4	0.0	5.15	0.76
0.8	-0.04	2.55	0.065		
0.93	0.16	2.83	-0.04		

TABLE IV (Contd.)

$w_5$					
$E_n$ (MeV)	$w_5$	$E_n$ (MeV)	$w_5$	$E_n$ (MeV)	$w_5$
0.0 <sup>b</sup>	0.0	1.05	0.02	3.62	0.18
0.15	-0.04	1.4	-0.05	3.95	-0.06
0.35	0.24	1.63	0.8	4.22	0.04
0.5	-0.02	1.95	0.02	4.7	-0.1
0.8	0.06	2.55	0.04	5.7	0.32
0.95	0.52	3.1	-0.1		

- a. Legendre coefficients are derived from data in Ref. 3. Angular distributions may be calculated from Eq. (3), however the coefficients listed above or interpolated values may not yield proper normalization. The computed distributions should be renormalized prior to use in scattering calculations.
- b. A "zero-energy" coefficient value is included in the table to provide a lower limit for interpolation.

TABLE V

Mean Free-Path for Neutron  
Elastic Scattering in Air<sup>a</sup>

$E_n$ (MeV)	$\lambda_E$ (cm)	$E_n$ (MeV)	$\lambda_E$ (cm)	$E_n$ (MeV)	$\lambda_E$ (cm)
0.05	2973	0.55	8097	2.0	11030
0.1	3185	0.6	9052	2.25	13780
0.15	3429	0.7	7984	2.5	14920
0.2	3714	0.8	9490	2.75	15740
0.25	4050	0.85	10330	3.0	13760
0.3	4454	0.9	9495	3.25	12140
0.35	4947	1.0	6854	3.5	11570
0.375	5236	1.1	6876	3.75	11700
0.4	5111	1.2	10260	4.0	14470
0.425	3115	1.3	7445	4.5	13680
0.45	3461	1.4	7712	5.0	16890
0.475	5200	1.5	9338		
0.5	6536	1.75	8568		

a. Values of  $\lambda_E$  computed from Eq. (11).

TABLE VI

Uranium Deposit Compositions Assumed for the  
Calculations in Section V

		<u>U-235 Enriched Deposit</u>		
U-234	content =	0.856%	}	Total mass 878 micrograms
U-235	content =	93.249%		
U-236	content =	0.332%		
U-238	content =	5.526%		

		<u>U-238 Enriched Deposit</u>		
U-235	content =	0.415%	}	Total mass 2398 micrograms
U-238	content =	99.585%		

U-234 and U-236 contents are negligible

TABLE VII

## Fission Cross Sections Used in the Present Work

U-234(n, f) Cross Sections

$E_n$ (MeV)	$\sigma_{F,234}$ (barns)	$E_n$ (MeV)	$\sigma_{F,234}$ (barns)	$E_n$ (MeV)	$\sigma_{F,234}$ (barns)
0.0	0.0 <sup>a</sup>	1.0	1.092 <sup>a</sup>	6.0	1.422 <sup>a</sup>
0.01	0.01 <sup>a</sup>	1.8	1.48 <sup>a</sup>	7.0	1.773 <sup>a</sup>
0.1	0.024 <sup>a</sup>	2.0	1.508 <sup>a</sup>	8.0	1.972 <sup>a</sup>
0.25	0.06 <sup>a</sup>	2.4	1.444 <sup>a</sup>	9.0	2.012 <sup>a</sup>
0.4	0.262 <sup>a</sup>	3.5	1.383 <sup>a</sup>	10.2	1.810 <sup>a</sup>
0.6	0.683 <sup>a</sup>	4.5	1.275 <sup>a</sup>	12.5	1.813 <sup>a</sup>
0.7	1.085 <sup>a</sup>	5.0	1.261 <sup>a</sup>	15.0	1.996 <sup>a</sup>
0.8	1.26 <sup>a</sup>	5.5	1.308 <sup>a</sup>		

U-235(n, f) Cross Sections

$E_n$ (MeV)	$\sigma_{F,235}$ (barns)	$E_n$ (MeV)	$\sigma_{F,235}$ (barns)	$E_n$ (MeV)	$\sigma_{F,235}$ (barns)
0.0	580.0 <sup>b</sup>	0.8	1.133 <sup>a</sup>	6.1	1.098 <sup>a</sup>
1.0x10 <sup>-6</sup>	65.0 <sup>b</sup>	0.85	1.15 <sup>a</sup>	6.3	1.164 <sup>a</sup>
0.001	8.05 <sup>b</sup>	0.95	1.218 <sup>a</sup>	6.8	1.413 <sup>a</sup>
0.003	4.99 <sup>b</sup>	1.0	1.235 <sup>a</sup>	7.2	1.552 <sup>a</sup>
0.01	3.21 <sup>b</sup>	1.5	1.247 <sup>a</sup>	7.6	1.634 <sup>a</sup>
0.0175	2.7 <sup>b</sup>	2.0	1.315 <sup>a</sup>	8.5	1.751 <sup>a</sup>
0.03	2.27 <sup>b</sup>	2.3	1.309 <sup>a</sup>	9.5	1.753 <sup>a</sup>
0.055	1.91 <sup>b</sup>	2.6	1.281 <sup>a</sup>	10.5	1.7 <sup>a</sup>
0.1	1.635 <sup>a</sup>	3.2	1.177 <sup>a</sup>	11.5	1.7 <sup>a</sup>
0.16	1.478 <sup>a</sup>	3.6	1.146 <sup>a</sup>	12.5	1.82 <sup>a</sup>
0.24	1.32 <sup>a</sup>	4.2	1.089 <sup>a</sup>	13.0	2.0 <sup>a</sup>
0.35	1.225 <sup>a</sup>	4.8	1.056 <sup>a</sup>	14.0	2.13 <sup>a</sup>
0.4	1.218 <sup>a</sup>	5.4	1.046 <sup>a</sup>	15.0	2.16 <sup>a</sup>
0.54	1.16 <sup>a</sup>	5.8	1.068 <sup>a</sup>		

TABLE VII (Contd.)

U-236(n, f) Cross Sections

$E_n$ (MeV)	$\sigma_{F,236}$ (barns)	$E_n$ (MeV)	$\sigma_{F,236}$ (barns)	$E_n$ (MeV)	$\sigma_{F,236}$ (barns)
0.0	0.0 <sup>a</sup>	2.0	0.828 <sup>a</sup>	7.0	1.43
0.7	0.027 <sup>a</sup>	2.4	0.882 <sup>a</sup>	7.85	1.73
0.9	0.292 <sup>a</sup>	2.8	0.872 <sup>a</sup>	9.0	1.84
1.2	0.61 <sup>a</sup>	5.0	0.868 <sup>a</sup>	11.5	1.72
1.4	0.69 <sup>a</sup>	5.5	0.822 <sup>a</sup>	13.5	1.65
1.6	0.688 <sup>a</sup>	6.0	0.903 <sup>a</sup>	15.0	1.62

U-238(n, f) Cross Sections

$E_n$ (MeV)	$\sigma_{F,238}$ (barns)	$E_n$ (MeV)	$\sigma_{F,238}$ (barns)	$E_n$ (MeV)	$\sigma_{F,238}$ (barns)
0.0	0.0 <sup>a</sup>	1.514	0.3458 <sup>c</sup>	4.47	0.5339
0.5	2.34x10 <sup>-4a</sup>	1.617	0.4169 <sup>c</sup>	5.08	0.5324
0.61	1.24x10 <sup>-3a</sup>	1.72	0.4472 <sup>c</sup>	5.33	0.5403
0.75	1.98x10 <sup>-3a</sup>	1.821	0.5122 <sup>c</sup>	6.0	0.618 <sup>a</sup>
0.85	5.87x10 <sup>-3a</sup>	1.914	0.5397 <sup>c</sup>	7.0	0.936 <sup>a</sup>
0.898	0.0123 <sup>c</sup>	2.0	0.5371 <sup>c</sup>	7.5	0.978 <sup>a</sup>
1.005	0.0163 <sup>c</sup>	2.51	0.5573 <sup>c</sup>	8.5	1.0 <sup>a</sup>
1.108	0.0273 <sup>c</sup>	3.08	0.525 <sup>c</sup>	10.0	0.974 <sup>a</sup>
1.205	0.0374 <sup>c</sup>	3.28	0.5242 <sup>c</sup>	12.0	0.995 <sup>a</sup>
1.306	0.0651 <sup>c</sup>	3.58	0.5352 <sup>c</sup>	13.5	1.098 <sup>a</sup>
1.401	0.1939 <sup>c</sup>	4.08	0.5336 <sup>c</sup>	15.0	1.25 <sup>a</sup>

a. Values obtained from ENDF/B-III evaluation [7].

b. Values obtained from Davey compilation [20,21].

c. Values calculated using ENDF/B-III values of  $\sigma_{F,235}$  [6] and Meadows U-238 to U-235 fission cross section ratios [11].

## TABLE VIII

### Normal Parameter Set for Air Scattering Calculations with the Detailed Single Scattering Formulation Described in Section V

1. Total, elastic and inelastic scattering cross sections for nitrogen (Table I).
2. Elastic scattering angular distribution coefficients for nitrogen (Table III).
3. Total and elastic scattering cross sections for oxygen (Table II).
4. Elastic scattering angular distribution coefficients for oxygen (Table IV).
5. Fission cross sections for U-234, U-235, U-236 and U-238. (Table VII).
6. Uranium deposit masses and compositions. (Table VI).
7. Isotropic, monoenergetic neutron point source.
8. Geometric parameters (see Fig. 3):

$$\begin{aligned}d &= 5 \text{ cm} \\R_{\text{DISK}} &= 1.27 \text{ cm} \\R_{\text{A,MAX}} &= Z_{\text{A,MAX}} = 30 \text{ cm}\end{aligned}$$

TABLE IX

Variation of  $F_2$  with Thickness  
of a U-235 Enriched Deposit<sup>a</sup>

Thickness Multiple	Deposit Weight (gm)	$F_2/F_2$ (Standard)
0.001	$8.784 \times 10^{-7}$	0.965
0.01	$8.784 \times 10^{-6}$	1.079
0.1	$8.784 \times 10^{-5}$	0.995
0.5	$4.392 \times 10^{-4}$	1.057
1 <sup>b</sup>	$8.784 \times 10^{-4}$	1
2	$1.757 \times 10^{-3}$	1.027
5	$4.392 \times 10^{-3}$	1.014
10	$8.784 \times 10^{-3}$	0.973
100	$8.784 \times 10^{-2}$	1.083
1000	$8.784 \times 10^{-1}$	0.987


  
Realistic deposit thickness range

- a. Values of  $F_2$  were calculated via the techniques of Section V and using the parameters indicated in Table VIII except for the deposit thickness which was variable.
- b. The standard deposit is the 878.4 microgram U-235 enriched deposit described in Table VI.

TABLE X

The Effect of Neutron Source Kinematic Broadening on  $F_2^a$ U-235 Enriched Deposit

$A_2$ (amu)	$F_2$	
	$E_1 = 1$ MeV	$E_1 = 3$ MeV
2	$.1980 \times 10^{-2}$	$.1003 \times 10^{-2}$
5	$.1298 \times 10^{-2}$	$.8325 \times 10^{-3}$
10	$.1348 \times 10^{-2}$	$.7209 \times 10^{-3}$
20	$.1267 \times 10^{-2}$	$.7046 \times 10^{-3}$
50	$.1406 \times 10^{-2}$	$.9163 \times 10^{-3}$
100	$.1714 \times 10^{-2}$	$.7979 \times 10^{-3}$
Infinite	$.1644 \times 10^{-2}$	$.9055 \times 10^{-3}$

U-238 Enriched Deposit

$A_2$	$F_2$	
	$E_1 = 1$ MeV	$E_1 = 3$ MeV
2	$.5975 \times 10^{-3}$	$.5553 \times 10^{-3}$
5	$.6581 \times 10^{-3}$	$.7066 \times 10^{-3}$
10	$.6199 \times 10^{-3}$	$.8517 \times 10^{-3}$
20	$.8130 \times 10^{-3}$	$.8260 \times 10^{-3}$
50	$.7485 \times 10^{-3}$	$.8378 \times 10^{-3}$
100	$.8714 \times 10^{-3}$	$.8121 \times 10^{-3}$
Infinite	$.9975 \times 10^{-3}$	$.8649 \times 10^{-3}$

- a. Values of  $F_2$  were calculated via the techniques of Section V. Hypothetical two-body neutron producing reactions with  $Q = 0$  which are initiated by a projectile with mass equal to a neutron ( $A_1 = 1.009$  amu) were assumed. Various target nuclei with masses (in amu)  $A_2 = 2, 5, 10, 20, 50, 100$  and infinity were considered. The neutron emission was taken to be isotropic and other parameters required for the calculations described in Section V were taken from Table VIII.

TABLE XI

Sensitivity of  $F_2$  to the Assumed Elastic  
Scattering Angular Distributions for  
Nitrogen and Oxygen<sup>a</sup>

U-235 Enriched Deposit

Normal Oxygen Distribution

$E_1$ (MeV)	Normal Nitrogen Distr.	$F_2$	Isotropic Nitrogen Distr.
1.0	$.1644 \times 10^{-2}$		$.1664 \times 10^{-2}$
1.8	$.1390 \times 10^{-2}$		$.1500 \times 10^{-2}$
2.5	$.6691 \times 10^{-3}$		$.7951 \times 10^{-3}$
3.0	$.9055 \times 10^{-3}$		$.9284 \times 10^{-3}$
3.5	$.1323 \times 10^{-2}$		$.1072 \times 10^{-2}$
5.0	$.8964 \times 10^{-3}$		$.8587 \times 10^{-3}$

Normal Nitrogen Distribution

$E_1$ (MeV)	Normal Nitrogen Distr.	$F_2$	Isotropic Oxygen Distr.
0.45	$.2880 \times 10^{-2}$		$.3933 \times 10^{-2}$
1.0	$.1644 \times 10^{-2}$		$.1607 \times 10^{-2}$
1.8	$.1390 \times 10^{-2}$		$.1510 \times 10^{-2}$
3.5	$.1323 \times 10^{-2}$		$.1208 \times 10^{-2}$
4.5	$.9422 \times 10^{-3}$		$.1463 \times 10^{-2}$

TABLE XI (Contd.)

U-238 Enriched Deposit

## Normal Oxygen Distribution

$E_1$ (MeV)	Normal Nitrogen Distr.	$F_2$	Isotropic Nitrogen Distr.
1.0	$.9975 \times 10^{-3}$		$.1008 \times 10^{-2}$
1.8	$.9673 \times 10^{-3}$		$.8453 \times 10^{-3}$
2.5	$.6568 \times 10^{-3}$		$.6878 \times 10^{-3}$
3.0	$.8649 \times 10^{-3}$		$.1129 \times 10^{-2}$
3.5	$.1312 \times 10^{-2}$		$.1016 \times 10^{-2}$
5.0	$.7637 \times 10^{-3}$		$.7266 \times 10^{-3}$

## Normal Nitrogen Distribution

$E_1$ (MeV)	Normal Nitrogen Distr.	$F_2$	Isotropic Nitrogen Distr.
0.45	$.2814 \times 10^{-2}$		$.3364 \times 10^{-2}$
1.0	$.9975 \times 10^{-3}$		$.8696 \times 10^{-3}$
1.8	$.9673 \times 10^{-3}$		$.9059 \times 10^{-3}$
3.5	$.1312 \times 10^{-2}$		$.1272 \times 10^{-2}$
4.5	$.8446 \times 10^{-3}$		$.8709 \times 10^{-3}$

- a. Values of  $F_2$  were calculated via the techniques of Section V. The parameters indicated in Table VIII were employed except for the substitution of isotropic elastic scattering angular distributions for nitrogen and oxygen where indicated.

TABLE XII

Coefficients for the Neutron Source Distributions  
Corresponding to the  ${}^7\text{Li}(p,n){}^7\text{Be}$  Reaction<sup>a</sup>

First-Group Neutrons (Q = -1.644 MeV)

Proton Energy (MeV)	w <sub>1</sub>	w <sub>2</sub>	w <sub>3</sub>	w <sub>4</sub>
2.8	1.19	0.5687	0.1619	0
3.0	1.113	0.4518	0.1075	0
3.2	1.054	0.4437	0.1121	0
3.4	0.9617	0.4044	0.1044	0
3.6	0.8843	0.3655	0.4093	-0.1598 x 10 <sup>-1</sup>
3.8	0.7795	0.3440	0.7762 x 10 <sup>-2</sup>	-0.3394 x 10 <sup>-1</sup>
4.0	0.6877	0.3714	0.1662 x 10 <sup>-2</sup>	-0.4365 x 10 <sup>-1</sup>
4.2	0.6097	0.4622	-0.6456 x 10 <sup>-1</sup>	-0.9487 x 10 <sup>-1</sup>
4.4	0.5802	0.5519	-0.3219 x 10 <sup>-1</sup>	-0.8957 x 10 <sup>-1</sup>
4.6	0.5612	0.6674	0.4624 x 10 <sup>-1</sup>	-0.6359 x 10 <sup>-1</sup>
4.8	0.5207	0.6743	0.1318	-0.1948 x 10 <sup>-1</sup>
5.0	0.4674	0.7297	0.3098	0.6363 x 10 <sup>-1</sup>

TABLE XII (Contd.)

Second Group Neutrons (Q = -2.079 MeV)

Proton Energy (MeV)	$w_1$	$w_2$	$w_3$	$w_4$
3.2	0.38	-0.1695	-0.1773	$-0.7445 \times 10^{-1}$
3.4	0.2859	-0.1582	-0.1427	$-0.5812 \times 10^{-1}$
3.6	0.1832	$-0.443 \times 10^{-1}$	$-0.4813 \times 10^{-3}$	$-0.495 \times 10^{-2}$
3.8	0.114	$0.517 \times 10^{-1}$	$0.7592 \times 10^{-2}$	$0.1545 \times 10^{-1}$
4.0	-0.3831	0.2217	$-0.6469 \times 10^{-1}$	$0.755 \times 10^{-3}$
4.2	$-0.4815 \times 10^{-3}$	0.223	$-0.2205 \times 10^{-2}$	$-0.5722 \times 10^{-1}$
4.4	$-0.3763 \times 10^{-1}$	0.2364	$-0.6162 \times 10^{-2}$	$-0.6 \times 10^{-1}$
4.6	$-0.9986 \times 10^{-1}$	0.2952	$0.2167 \times 10^{-1}$	$-0.5371 \times 10^{-1}$
4.8	$-0.7796 \times 10^{-1}$	0.3609	$-0.6173 \times 10^{-1}$	-0.1084
5.0	$-0.7609 \times 10^{-1}$	0.4322	$-0.8369 \times 10^{-1}$	-0.1287

- a. Laboratory angular distributions for the  ${}^7\text{Li}(p,n){}^7\text{Be}$  reaction were obtained by transformation of the center-of-momentum distributions given by Elbakr et al. [11]. These distributions were fitted with the Legendre expansion

$$S(\theta_{\text{LAB}}) = 1 + \sum_{k=1}^n w_k P_k(\cos \theta_{\text{LAB}}).$$

A fourth-order expansion( $n=4$ ) was found to be adequate for this purpose.

## FIGURE CAPTIONS

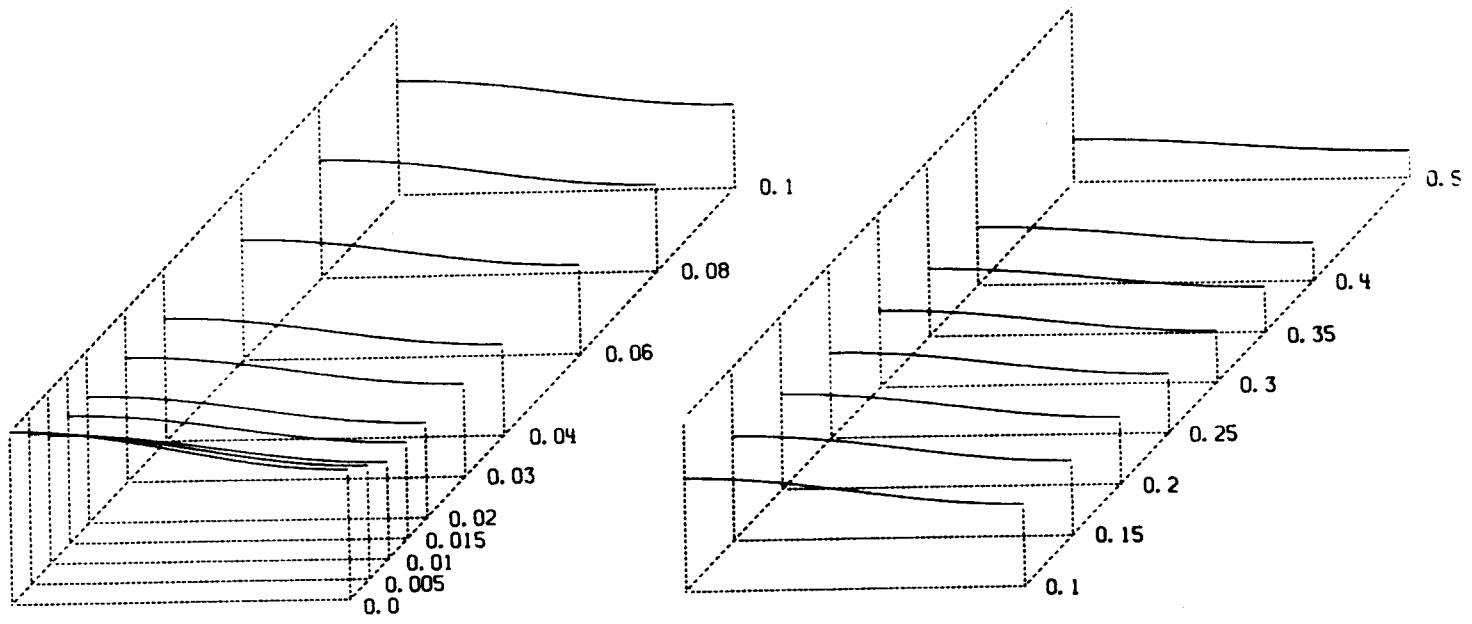
- Fig. 1. Laboratory neutron elastic-scattering angular distributions for nitrogen computed from the Legendre coefficients given in Table III. The curves were all plotted using the same ordinate scale. The neutron energies shown are in MeV. The negative cross sections appearing at 2.5 MeV are nonphysical and such values were excluded from the scattering calculations. (ANL Neg. No. 116-1904).
- Fig. 2. Laboratory neutron elastic-scattering angular distributions for oxygen computed from the Legendre coefficients given in Table IV. The curves were all plotted using the same ordinate normalization. The neutron energies shown are in MeV. Notice the strong forward scattering near the 0.44 MeV resonance. (ANL Neg. No. 116-1912).
- Fig. 3. Schematic diagram of a thin uranium deposit in a fission chamber which is placed near a point source of neutrons. (ANL Neg. No. 116-1909).
- Fig. 4. The solid curve is a plot of  $F_0$  computed from Eq. (10) using values of  $\lambda_E$  from Table V for  $d = 5$  cm. The individual points are values of  $F_1$  for  $d = 5$  cm and  $R_{\text{DISK}} = 1.27$  cm computed via the Monte-Carlo techniques described in Section IV. (ANL Neg. No. 116-1906).
- Fig. 5. Plot of the ratio  $F_1/F_0$  computed from Eqs. (10) and (19) for several values of  $R_{A,\text{MAX}} (= Z_{A,\text{MAX}})$  with  $E_n = 1$  MeV,  $d = 5$  cm and  $R_{\text{DISK}} = 1.27$  cm. (ANL Neg. No. 116-1905).
- Fig. 6. Plot of the ratio  $F_1/F_0$  computed from Eqs. (10) and (19) for several values of  $d$  with  $E_n = 1$  MeV,  $R_{\text{DISK}} = 1.27$  cm and  $R_{A,\text{MAX}} = Z_{A,\text{MAX}} > 10 d$ . (ANL Neg. No. 116-1913).

- Fig. 7. Plot of the average angle of incidence  $\bar{\theta}_I$  for several values of  $d$  with  $E_n = 1$  MeV,  $R_{\text{DISK}} = 1.27$  cm and  $R_{A,\text{MAX}} = Z_{A,\text{MAX}} > 10 d$ . Computations were performed according to procedures described in Section IV. (ANL Neg. No. 116-1908).
- Fig. 8. Plots of the neutron angle-of-incidence distributions for several values of  $d$  with  $E_n = 1$  MeV,  $R_{\text{DISK}} = 1.27$  cm and  $R_{A,\text{MAX}} = Z_{A,\text{MAX}} > 10 d$ . Computations were performed according to procedures described in Section IV. The distribution function becomes nearly linear when  $d/R_{\text{DISK}}$  becomes large and the effects of finite uranium deposit size are negligible. (ANL Neg. No. 116-1911).
- Fig. 9. Plots of the neutron arrival-time distributions for several neutron energies with  $R_{\text{DISK}} = 1.27$  cm,  $d = 5$  cm and  $R_{A,\text{MAX}} = Z_{A,\text{MAX}} > 10 d$ . Computations were performed according to procedures described in Section IV. (ANL Neg. No. 116-1910).
- Fig.10. Plot of  $F_0$  and of  $F_2$  for a U-235 enriched deposit and for a U-238 enriched deposit. Calculations were performed according to the methods of Sections III and V using the parameters indicated in Table VIII. (ANL Neg. No. 116-1907).
- Fig.11. Plots of the relative number of fissions vs. the energy of neutrons incident upon a U-235 enriched deposit. Notice the appearance of an inelastic contribution in the plot for 5 MeV primary energy. Calculations were performed with the methods of Section V and the parameters indicated in Table VIII. (ANL Neg. No. 116-1915).
- Fig.12. Plots of the relative number of fissions vs. the energy of neutrons incident upon a U-238 enriched deposit. Notice the appearance of an inelastic contribution in the plot for 5 MeV primary energy. Calculations were performed with the methods of Section V and the parameters indicated in Table VIII. (ANL Neg. No. 116-1914).

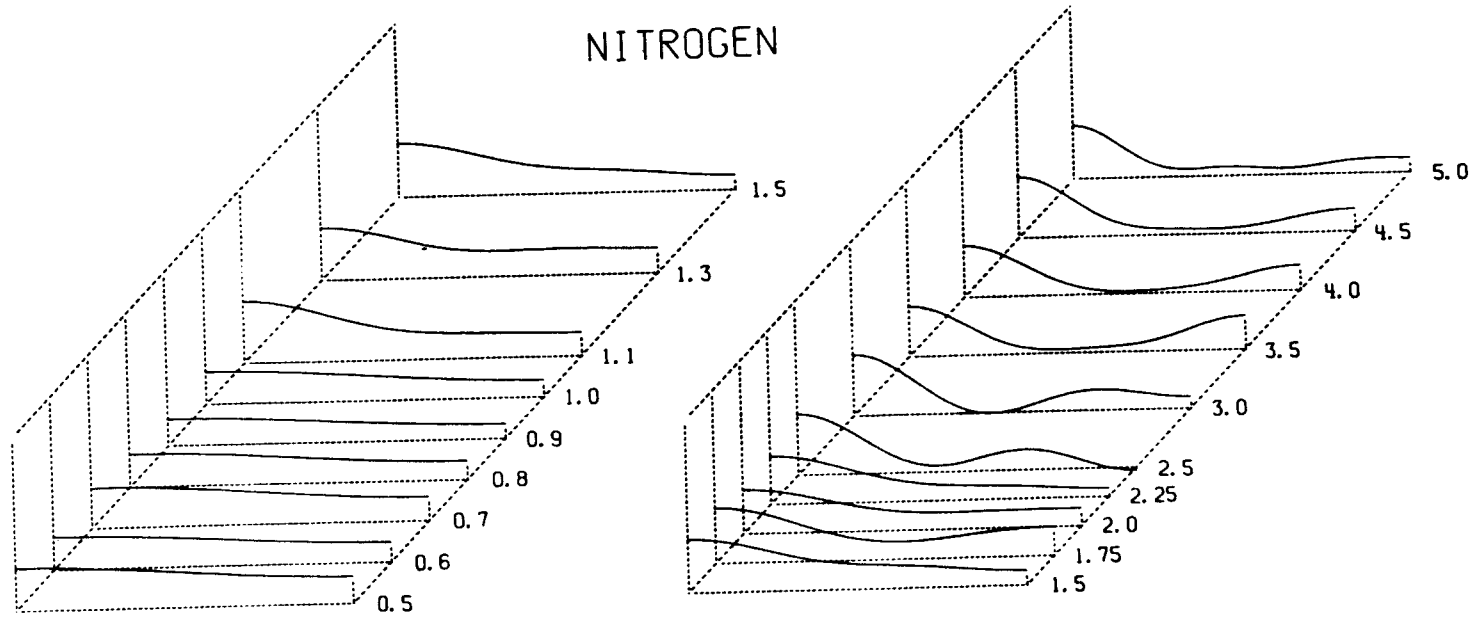
Fig.13. Dependence of  $F_2$  on the shape of the neutron source distribution. The insert figures show the neutron source distribution shapes  $S(\theta_{LAB}) = 1 + w_1 P_1(\cos \theta_{LAB})$  for  $w_1 = -1, 0$  and  $1$ . Calculations were made for a primary energy of 1 MeV and additional parameters of the calculations were as indicated in Table VIII. The calculational procedure is described in Section V. Notice that  $F_2$  is very sensitive to the value of  $w_1$  for  $-1 \leq w_1 < 0$  (back angle peaking). (ANL Neg. No. 116-1903).

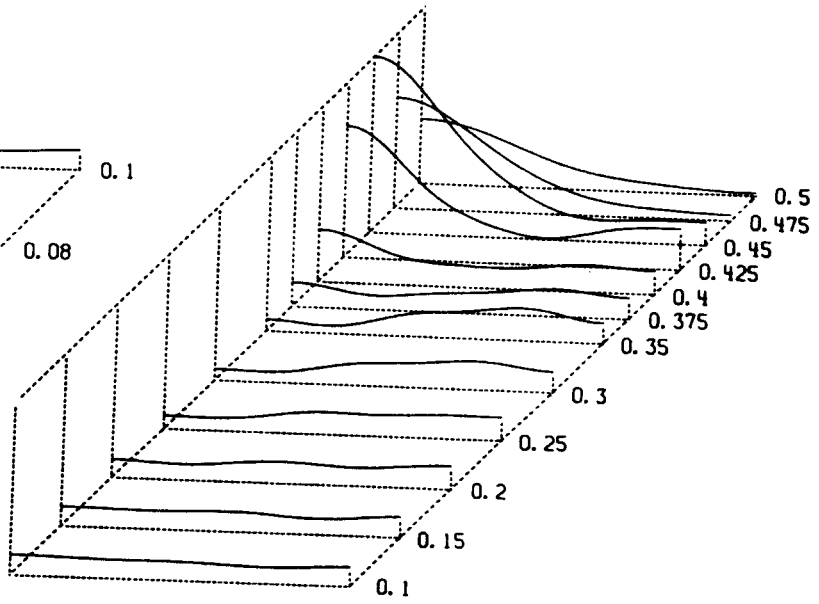
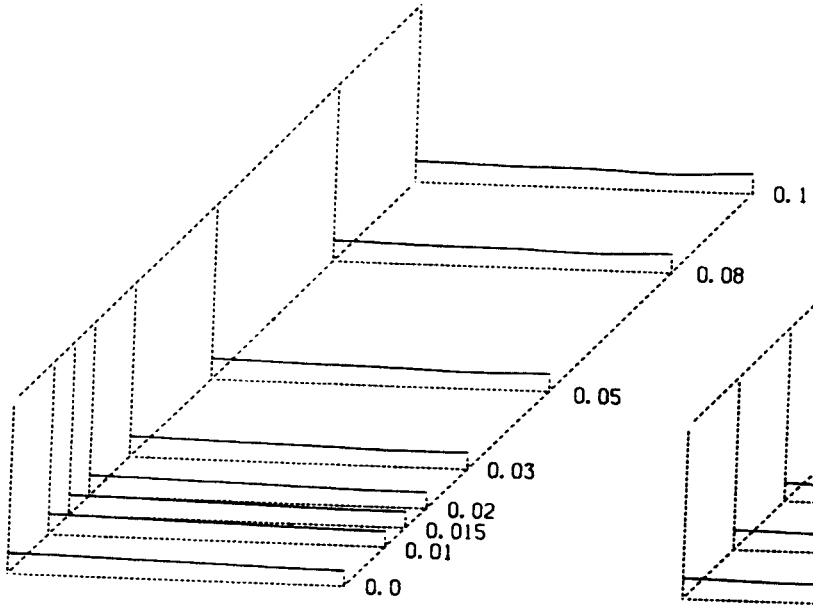
Fig.14. Plot of  $F_0$  and of  $F_2$  for a U-235 enriched deposit. Calculations were made assuming an isotropic, monoenergetic neutron source as well as the  $Q = -1.644$  MeV and  $Q = -2.079$  MeV groups from the  ${}^7\text{Li}(p,n){}^7\text{Be}$  reaction. Other parameters required for these calculations were obtained from Table VIII and the methods of Sections III and IV were used in the analysis. (ANL Neg. No. 116-1916).

Fig.15. Plot of  $F_0$  and of  $F_2$  for a U-238 enriched deposit. Calculations were made assuming an isotropic, monoenergetic neutron source as well as the  $Q = -1.644$  MeV and  $Q = -2.079$  MeV groups from the  ${}^7\text{Li}(p,n){}^7\text{Be}$  reaction. Other parameters required for these calculations were obtained from Table VIII and the methods of Sections III and IV were used in the analysis. (ANL Neg. No. 116-1917).

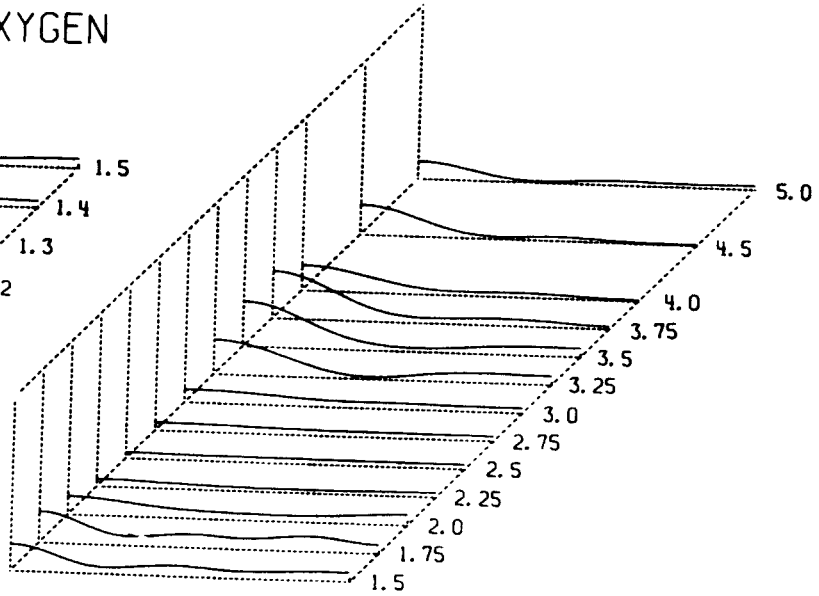
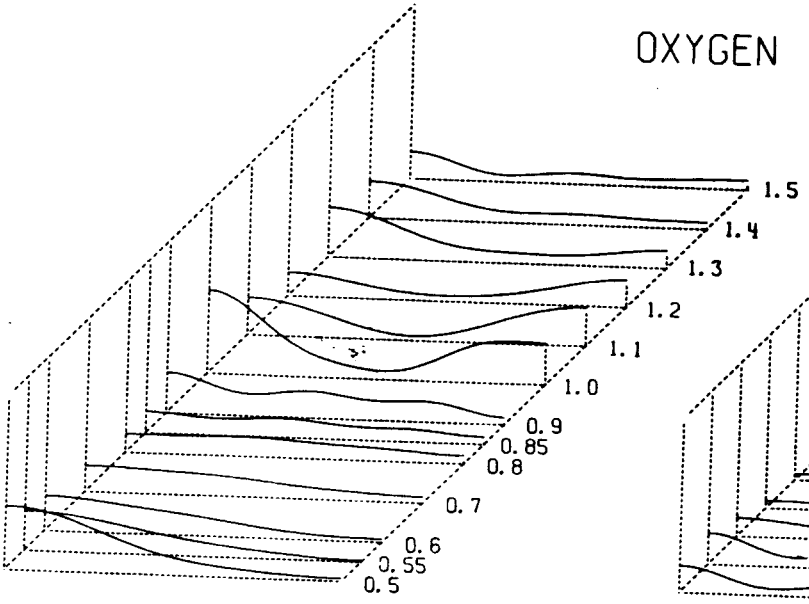


NITROGEN





OXYGEN



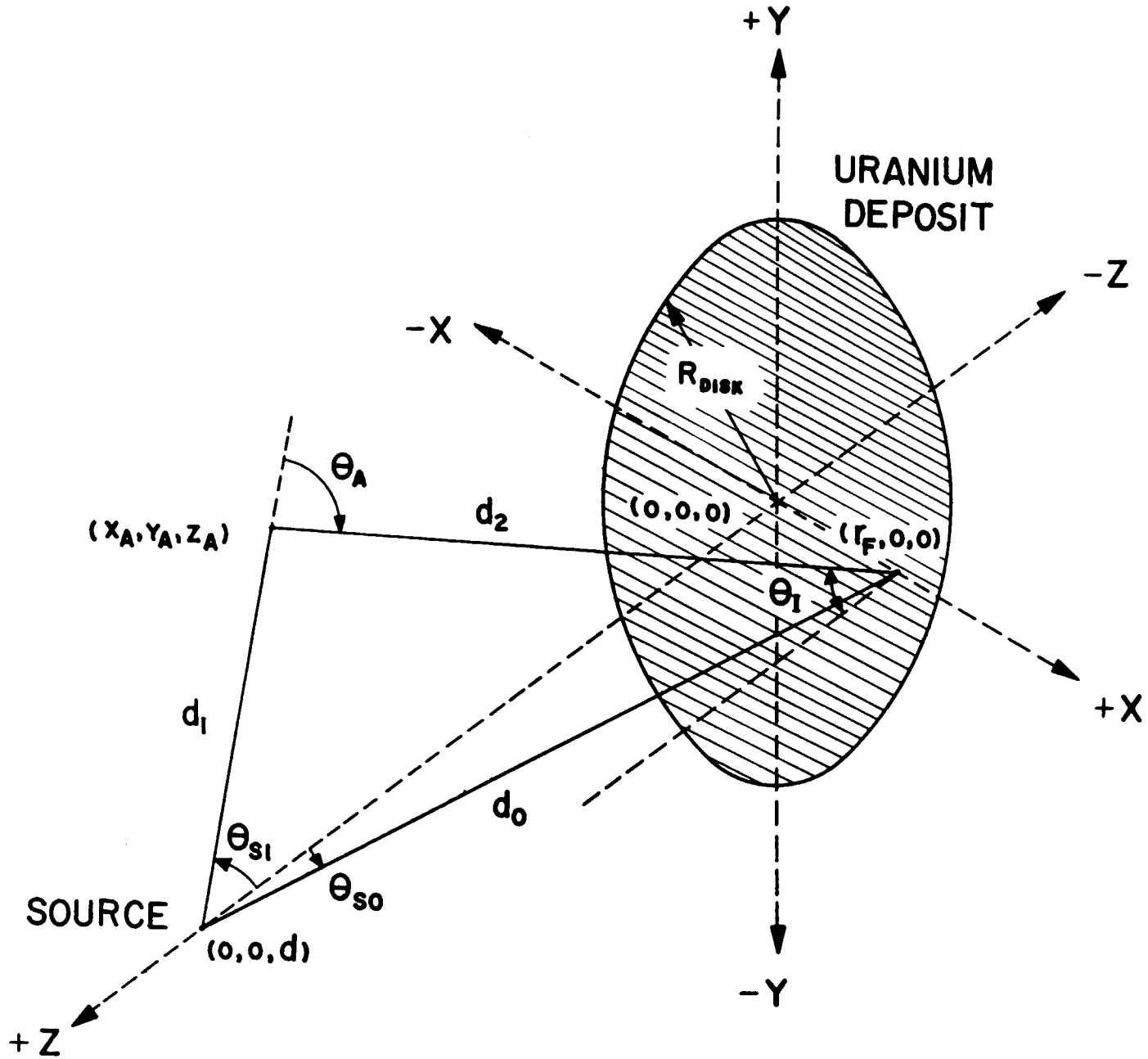


Fig. 3

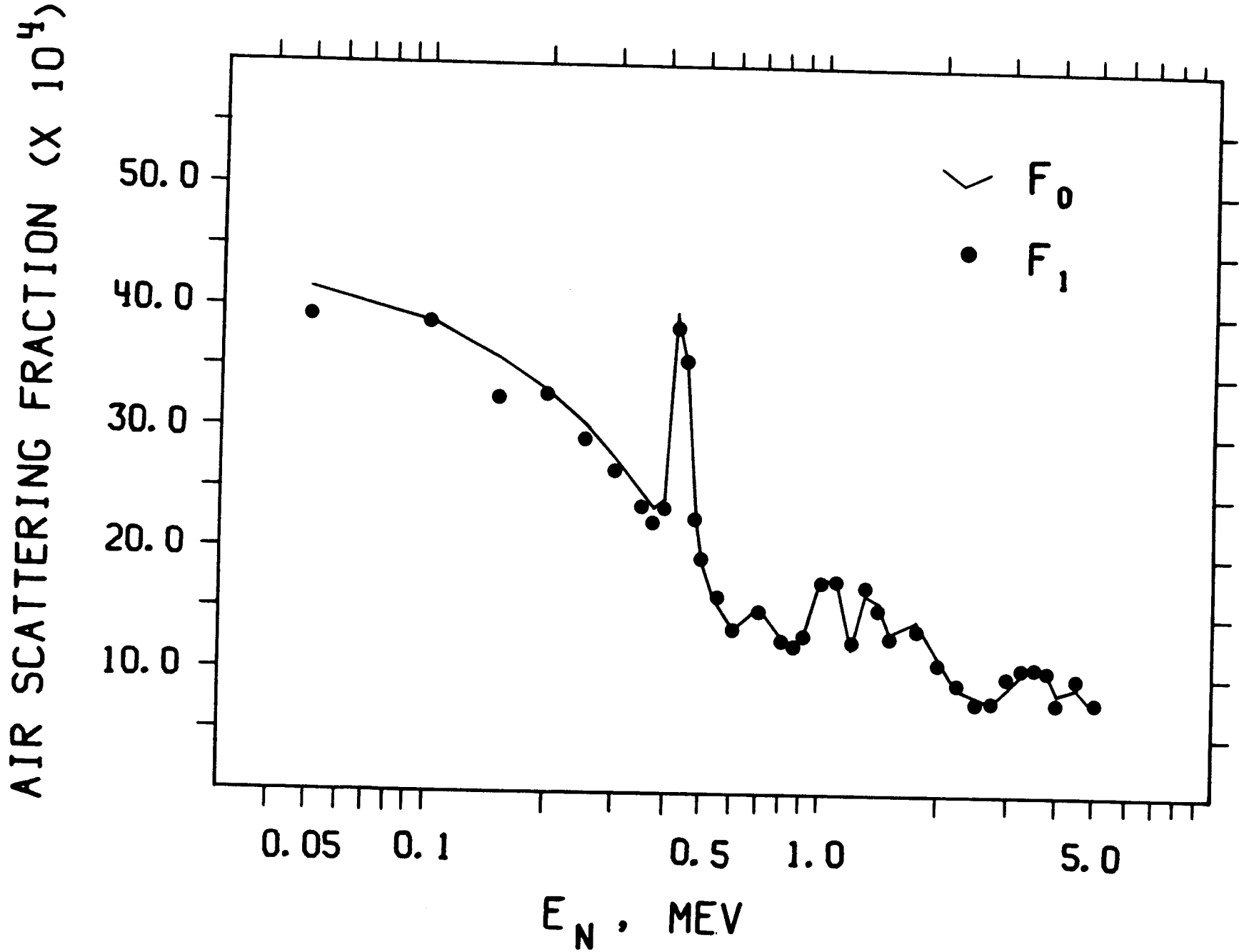


Fig. 4

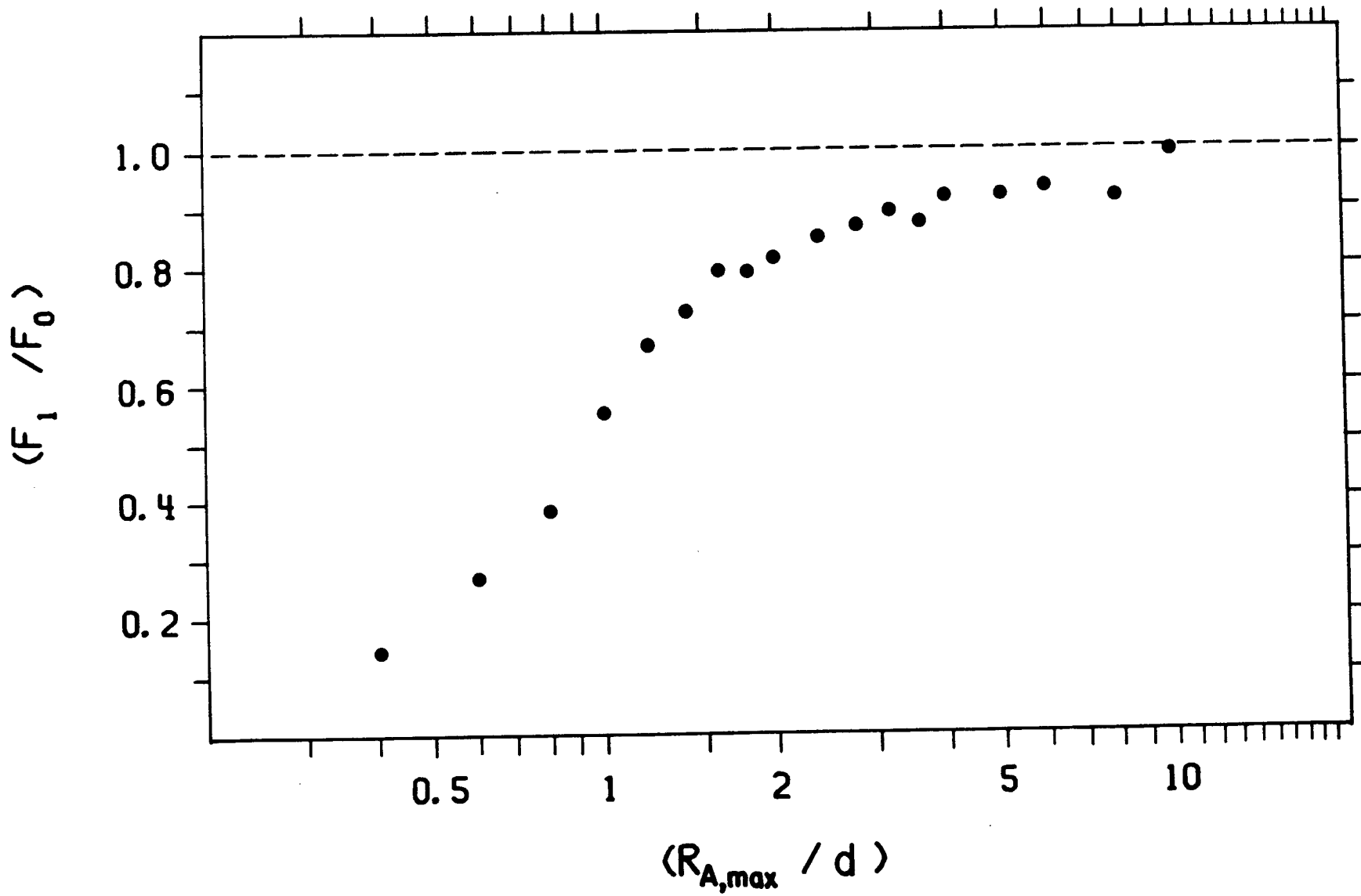


Fig. 5

$(F_1 / F_0)$

1.6  
1.4  
1.2  
1.0  
0.8  
0.6

SUPPRESSED ZERO

0.2 0.5 1 2 5 10 20 50

$(d / R_{\text{DISK}})$

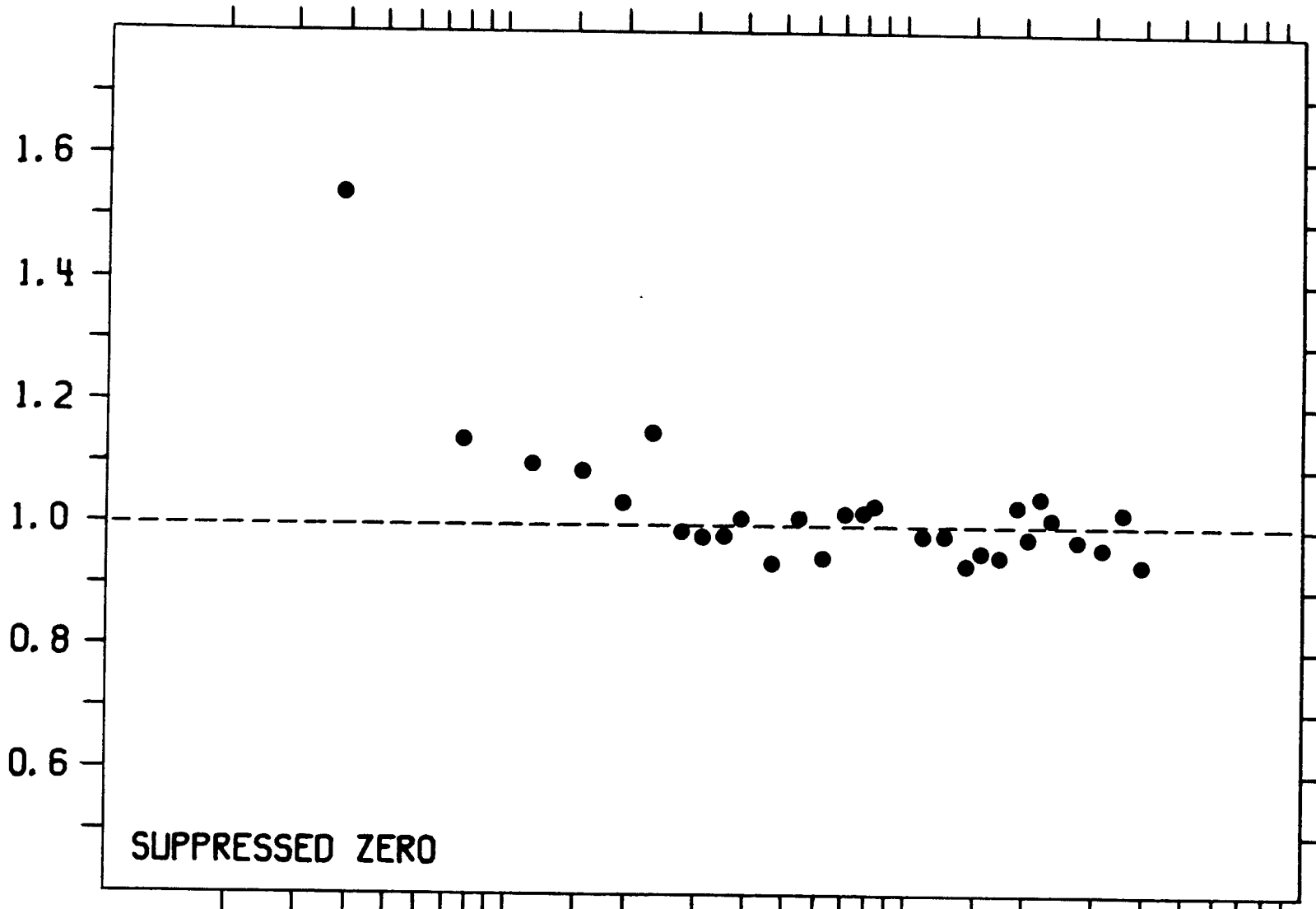


Fig. 6

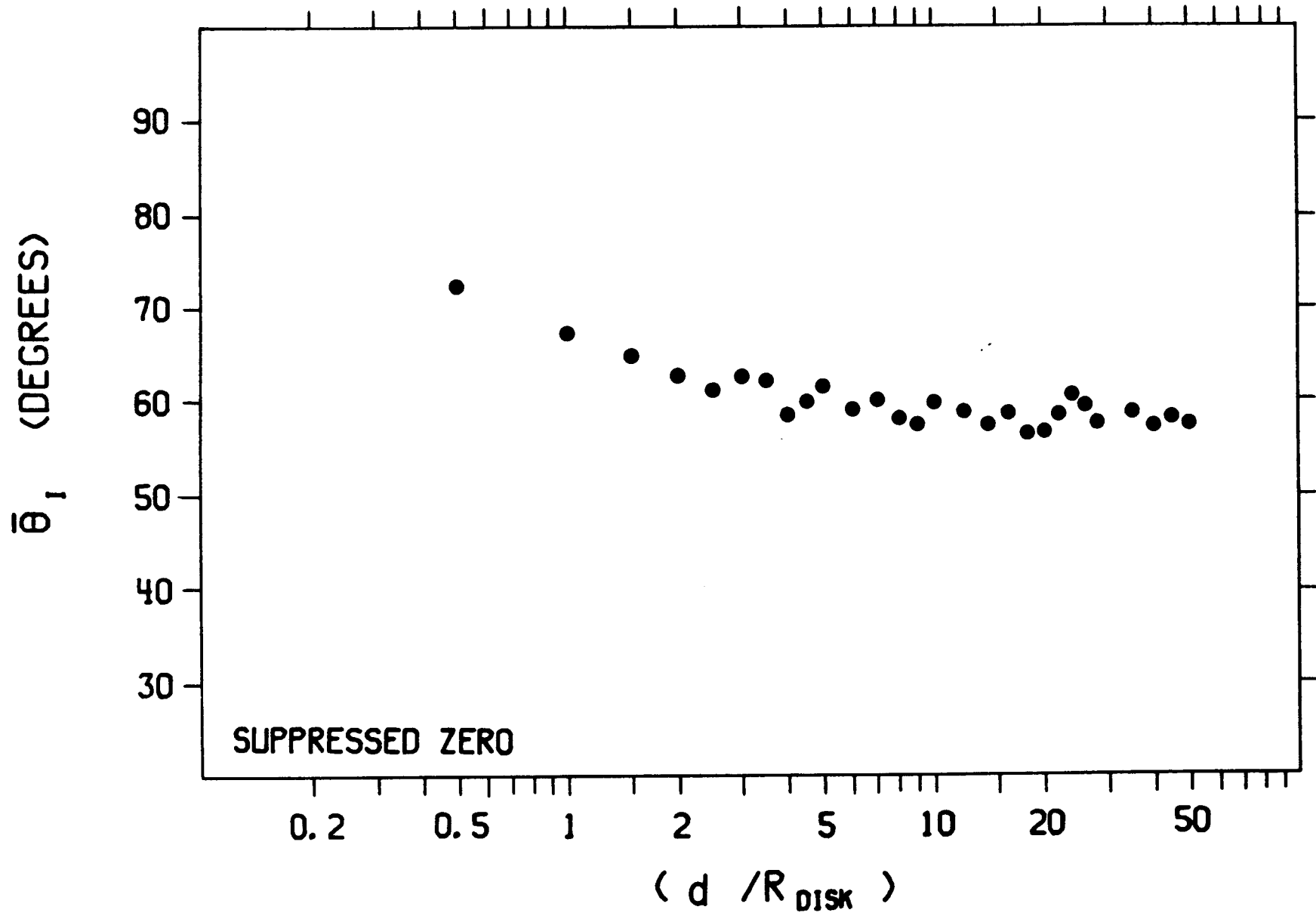
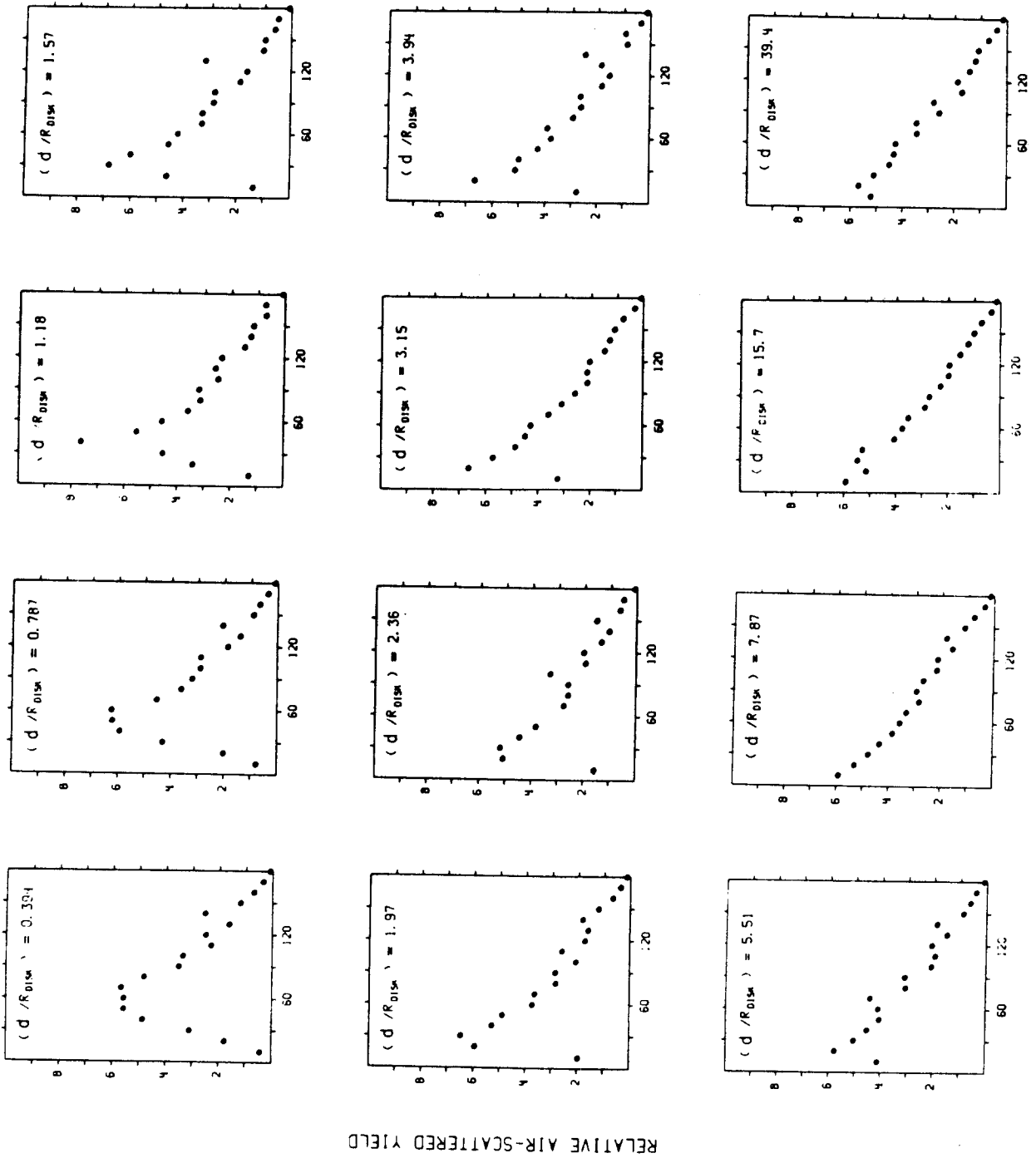


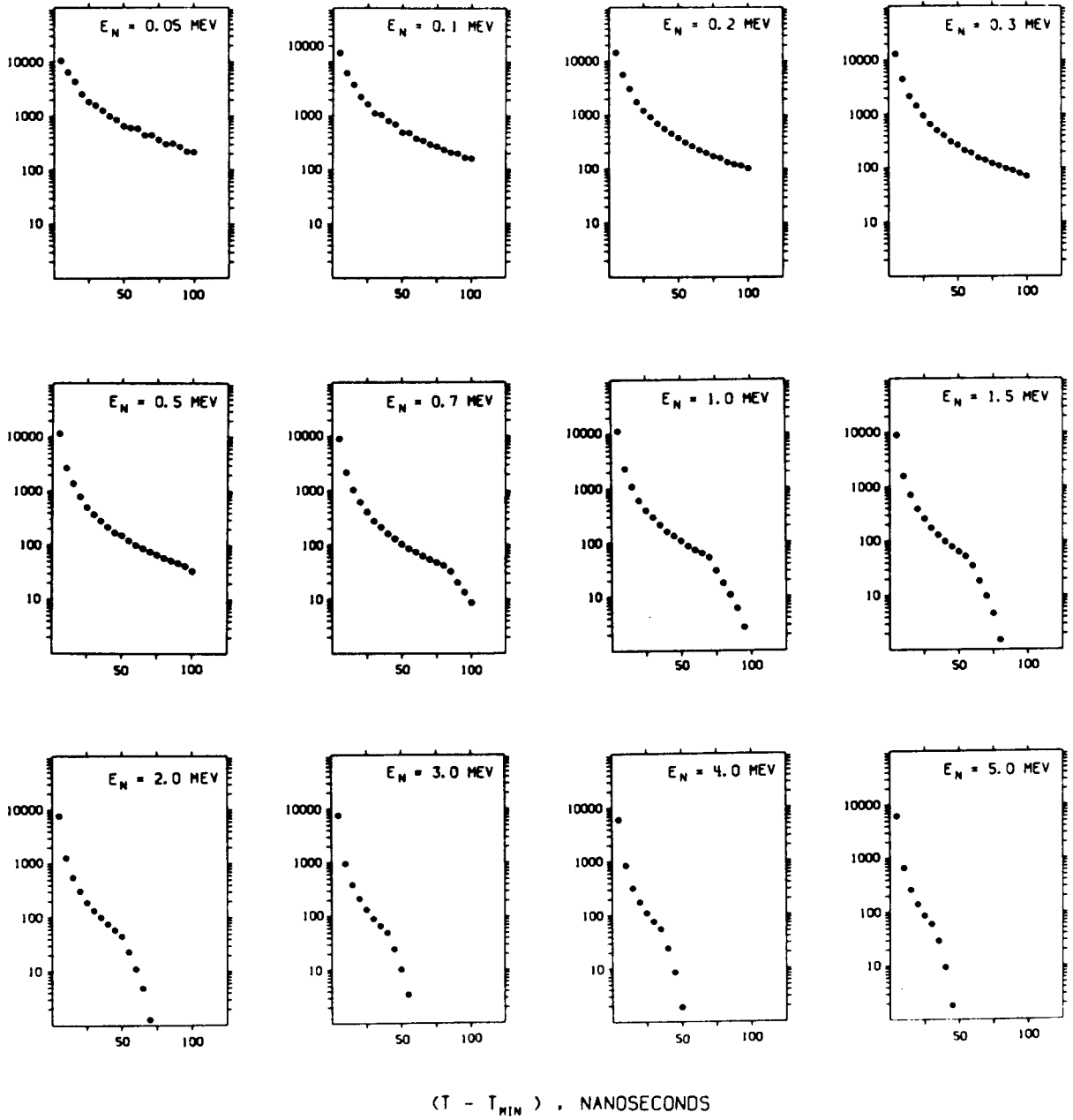
Fig. 8



$\theta_1$ , DEGREES

Fig. 9

RELATIVE AIR-SCATTERED YIELD



AIR SCATTERING FRACTION ( $\times 10^4$ )

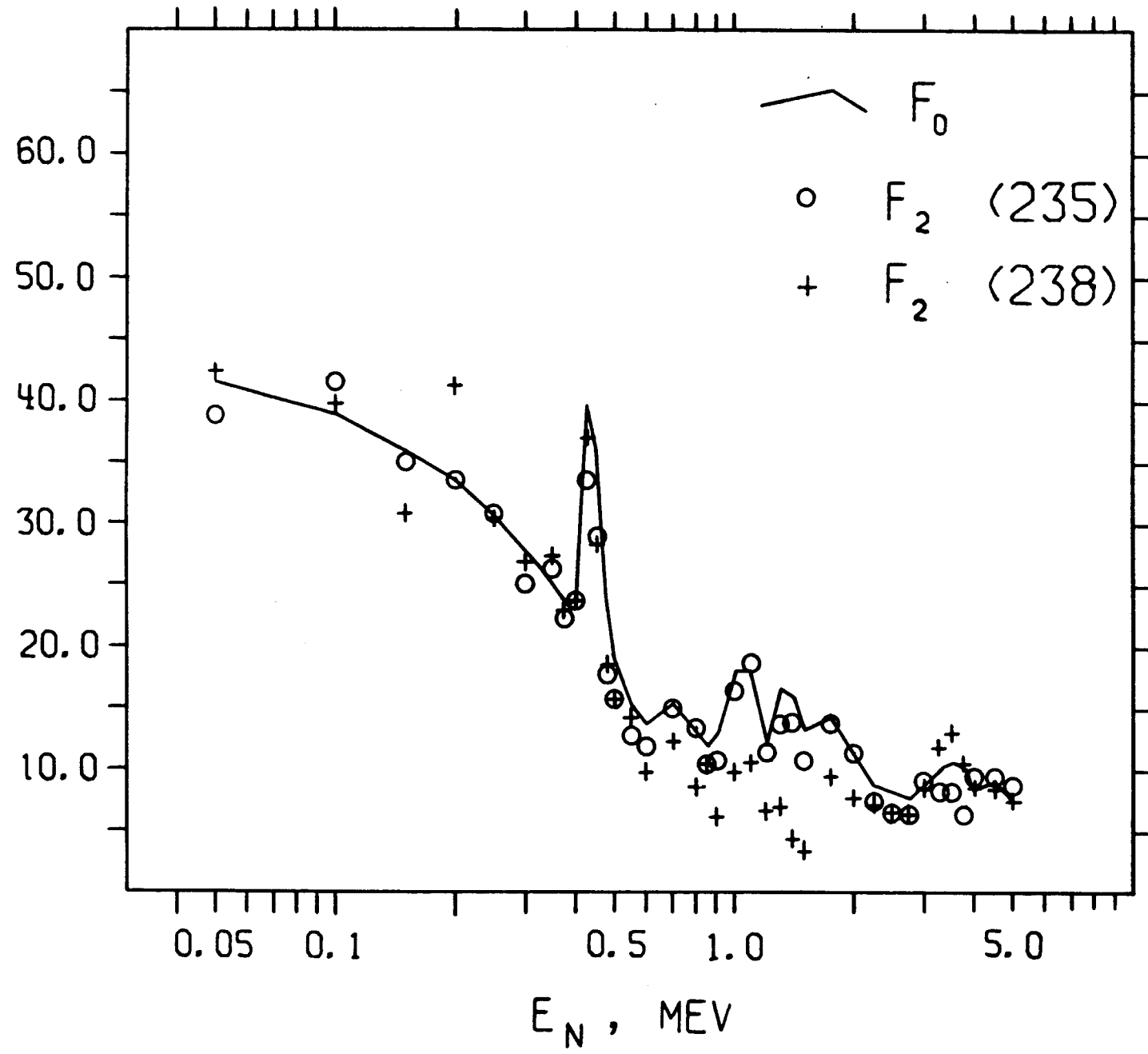
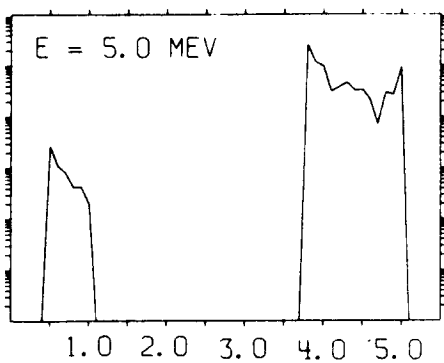
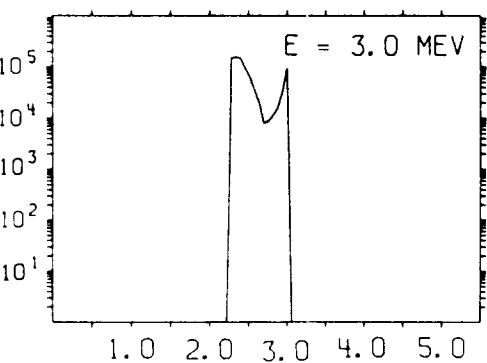
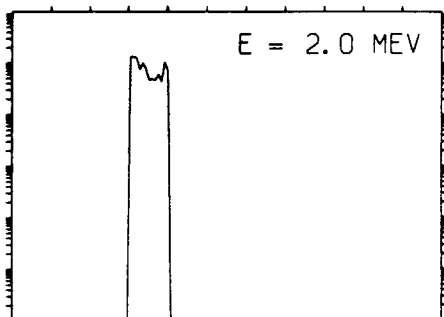
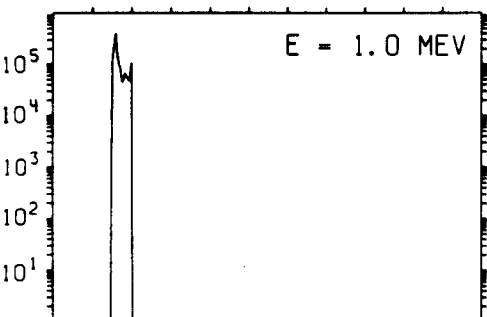
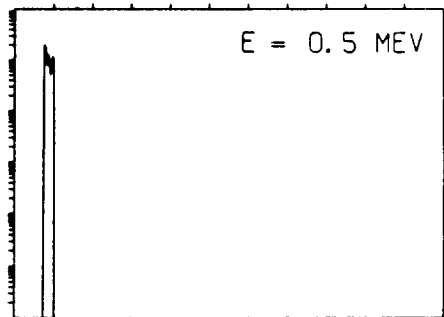
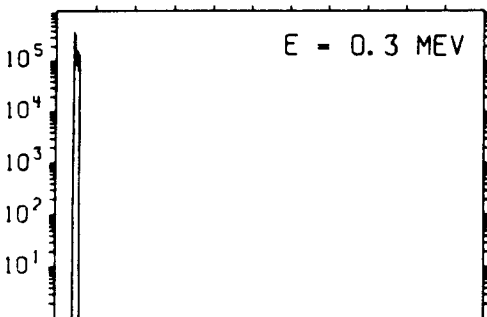
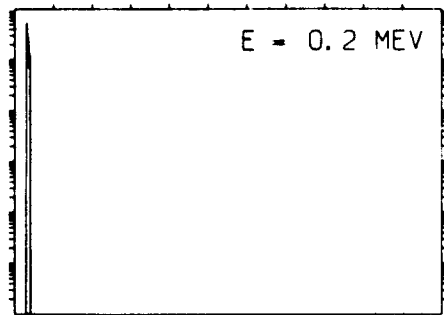
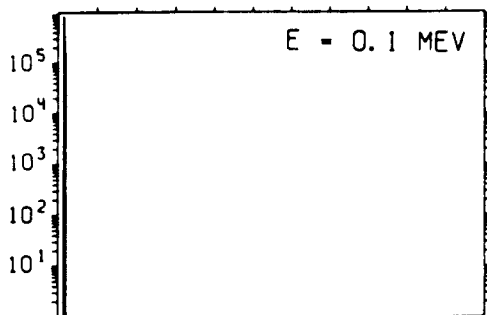


Fig. 10

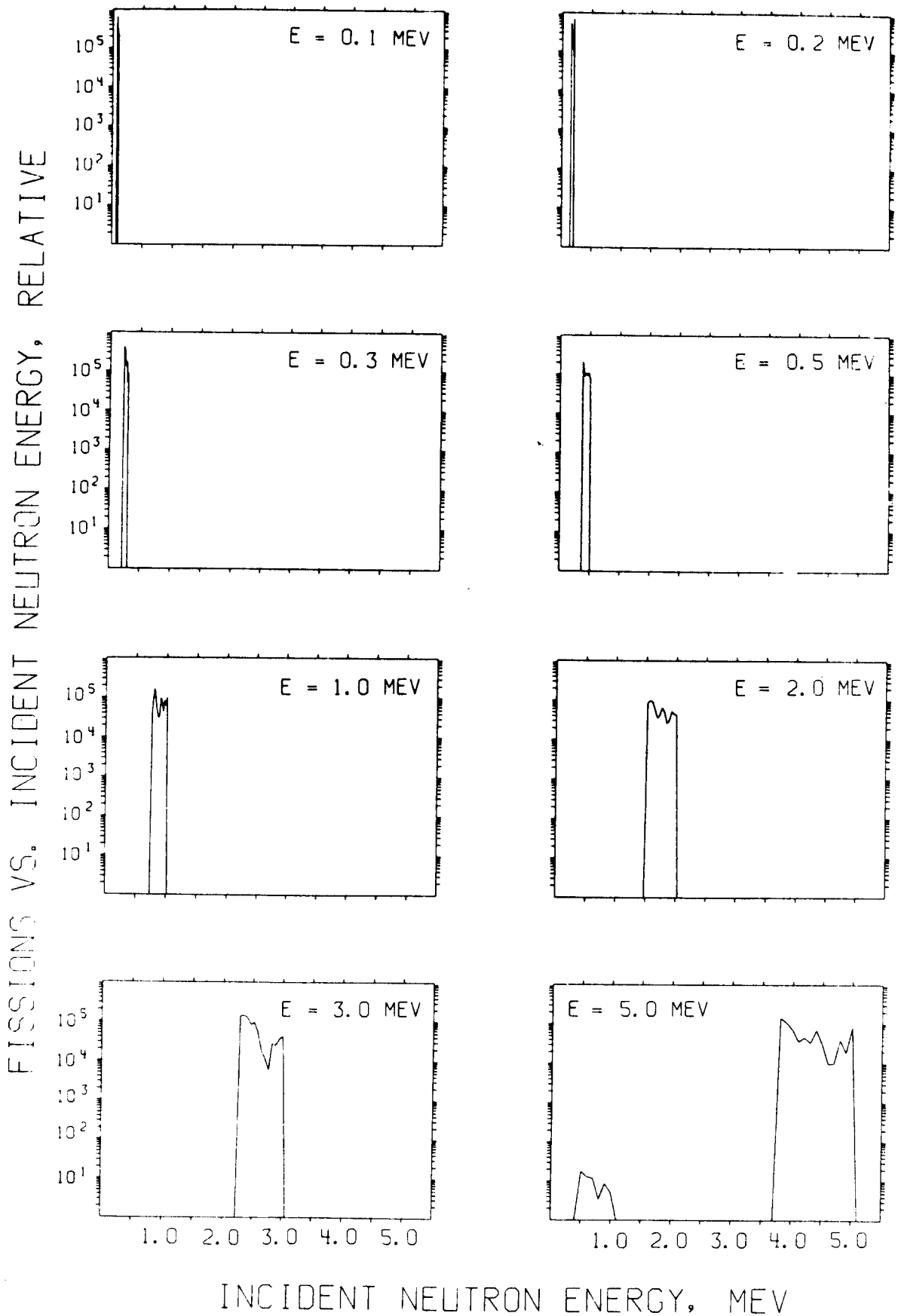
Fig.11

FISSIONS VS. INCIDENT NEUTRON ENERGY, RELATIVE



INCIDENT NEUTRON ENERGY, MEV

Fig.12



# AIR SCATTERING FRACTION

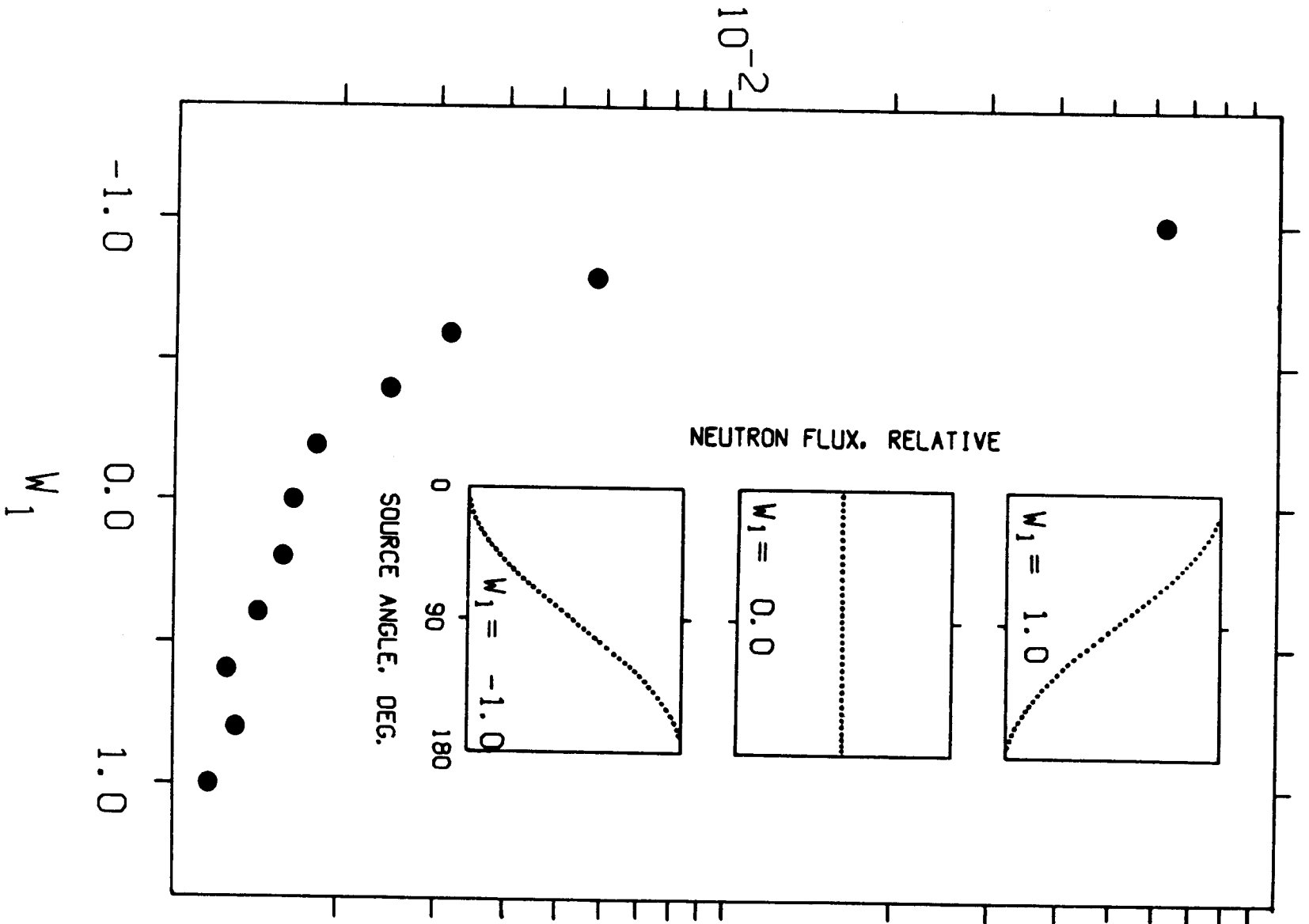


Fig. 13

RATIO OF AIR-SCATTERED  
TO PRIMARY NEUTRONS ( $\times 10^3$ )

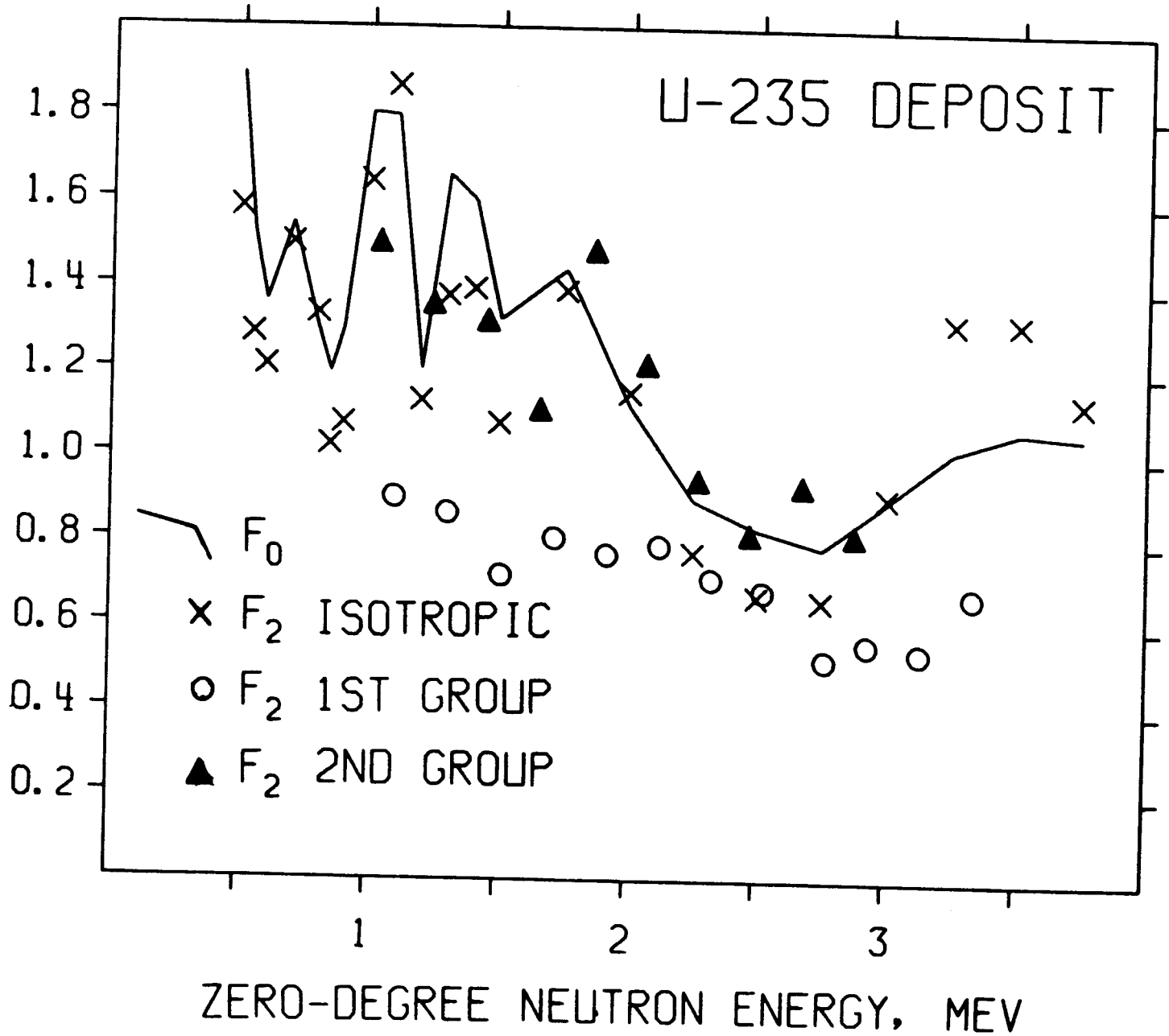


Fig. 14

Fig.15

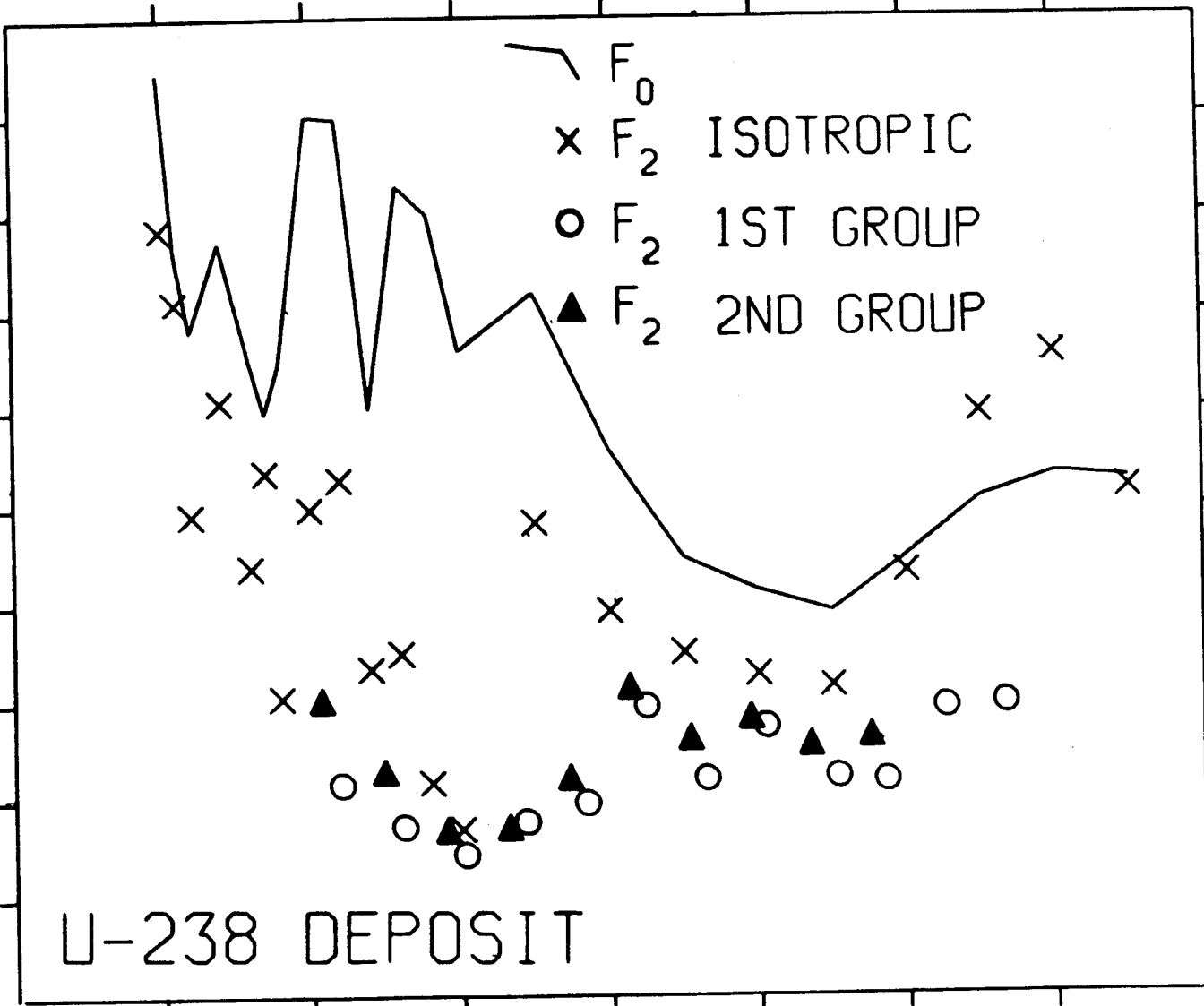
RATIO OF AIR-SCATTERED  
TO PRIMARY NEUTRONS ( $\times 10^3$ )

1.8  
1.6  
1.4  
1.2  
1.0  
0.8  
0.6  
0.4  
0.2

U-238 DEPOSIT

$F_0$   
 $\times F_2$  ISOTROPIC  
 $\circ F_2$  1ST GROUP  
 $\blacktriangle F_2$  2ND GROUP

ZERO-DEGREE NEUTRON ENERGY, MEV



## APPENDIX I

### Listing of FORTRAN IV Code AIRSC1

This program was used in conjunction with an SEL 840 MP computer equipped with an extended arithmetic unit to perform the calculations discussed in Section IV. The interpolation tables included in the input provide basic physical data, such as cross sections, which are required for the calculations. Unit 1 refers to a teletype I/O device, Unit 4 is a card reader while Unit 5 is a line printer.

AIRSC1

DIMENSION ENE(50),SIGNE(50),EØE(50),SIGØE(50),THI(36),YSA(36),RA  
1(36),T(20),YST(21),RTIME(21)  
DATA ATMDN,ATMDØ,AVØG,PI1,PI2/.4034E+20,.1066E+20,.1E-23,3.14159  
1.23318/

VALUE(Z,VMIN,VMAX)=VMIN+Z\*(VMAX-VMIN)

CONTROL

1 READ(4,2) IC  
2 FØRMT(I1)  
GØ TØ(10,20,30,40),IC  
10 PAUSE  
GØ TØ 1

READ INTERPOLATION TABLES

20 READ(4,31) NNE  
READ(4,21) (ENE(I),SIGNE(I),I=1,NNE)  
21 FØRMT(8E10,4)  
READ(4,31) NØE  
READ(4,21) (EØE(I),SIGØE(I),I=1,NØE)

READ AND WRITE BASIC PARAMETERS

30 READ(4,21) D,RDISK  
READ(4,31) MHIST,NHIST,NTIME,NANG  
31 FØRMT(16I5)  
READ(4,21) ZAMAX,RAMAX,TRANG  
WRITE(5,35) D,RDISK  
35 FØRMT(1H1,7HD,RDISK/2E10,4)  
WRITE(5,36) MHIST,NHIST,NTIME,NANG  
36 FØRMT(22HMIST,NHIST,NTIME,NANG/4I6)  
WRITE(5,37) ZAMAX,RAMAX,TRANG  
37 FØRMT(17HZAMAX,RAMAX,TRANG/3E10,4)  
WRITE(5,38)  
38 FØRMT(/5H.....)

READ AND WRITE E

40 READ(4,21) E  
WRITE(5,42) E  
42 FØRMT(1HE/E10,4)

CALCULATE MACROSCOPIC ELASTIC SCATTERING CROSS SECTION AND MEAN  
FREE PATH FOR ELASTIC SCATTERING

CALL INTRPL(ENE,ENE,SIGNE,E,VSNE)  
CALL INTRPL(NØE,EØE,SIGØE,E,VSØE)  
SIGME=AVØG\*(ATMDN\*VSNE+ATMDØ\*VSØE)  
FREE=1.0/SIGME

CALCULATE INCIDENT ANGLES THI(I)

JØ 48 I=1,NANG  
48 THI(I)=180.0\*FLØAT(I)/FLØAT(NANG)

C CALCULATE T(I) AND TMIN

C  
DO 50 I=1,NTIME  
50 T(I)=TRANG\*FLOAT(I)/FLOAT(NTIME)  
TMIN=TIME(E,D)

C  
C.....CALCULATE YDIR

C  
YDIR=0.0  
DO 100 IDIR=1,MHIST

C  
C  
SELECT RF AT RANDOM

C  
Z=RANF(-1)  
RF=VALUE(Z,0.0,RDISK)

C  
C  
CALCULATE THS AND DO

C  
THS=ATAN(RF/D)  
DO=D/COS(THS)

C  
100 YDIR=YDIR+(RF/DO/DO)

C  
C  
CALCULATE HISTORY AVERAGE

C  
YDIR=YDIR/FLOAT(MHIST)

C  
C.....CALCULATE YSA(I) AND YST(I)

C  
DO 105 I=1,NANG  
105 YSA(I)=0.0  
NBIN=NTIME+1  
DO 110 I=1,NBIN  
110 YST(I)=0.0  
SUMNTH=0.0  
SUMD=0.0

C  
DO 900 ISCAT=1,NHIST

C  
C  
SELECT RF,RA,ZA AND PHA AT RANDOM

C  
Z=RANF(-1)  
RF=VALUE(Z,0.0,RDISK)  
Z=RANF(-1)  
RA=VALUE(Z,0.0,RA MAX)  
Z=RANF(-1)  
ZA=VALUE(Z,-ZAMAX,ZAMAX)  
Z=RANF(-1)  
PHA=VALUE(Z,0.0,PI2)

C  
C  
CALCULATE XA,YA,D1 AND D2. SKIP TRIAL IF D1 OR D2 TOO SMALL

C  
XA=RA\*COS(PHA)  
YA=RA\*SIN(PHA)  
D1=SQRT(XA\*XA+YA\*YA+(ZA-D)\*(ZA-D))  
IF(D1-.1E-10) 900,900,120  
120 D2=SQRT((XA-RF)\*(XA-RF)+YA\*YA+ZA\*ZA)  
IF(D2-.1E-10) 900,900,130

C  
C  
CALCULATE THINC AND INDXA

```

C
130 CALL ANGLE(0.,0.,0.,0.,0.,D,RF,0.,0.,XA,YA,ZA,THINC)
    THINC=57.2957795*THINC
    INDXA=THINC*FLOAT(NANG)/180.001
    INDXA=INDXA+1
C
C
C    CALCULATE T1,T2 AND INDXT
    T1=TIME(E,D1)
    T2=TIME(E,D2)
    INDXT=(T1+T2-TMIN)*FLOAT(NTIME)/TRANG
    INDXT=INDXT+1
    IF(INDXT.GT.NBIN) INDXT=NBIN
C
    YLD=RA*RF/D1/D1/D2/D2
    SUMNTH=SUMNTH+YLD*THINC
    SUMD=SUMD+YLD
    YSA(INDXA)=YSA(INDXA)+YLD
    YST(INDXT)=YST(INDXT)+YLD
900 CONTINUE
C
C
C    MULTIPLY BY SIGME AND AIR PARAMETER SPACE VOLUME. CALCULATE
    HISTORY AVERAGES
    D0 905 I=1,NANG
905  YSA(I)=RAMAX*ZAMAX*SIGME*YSA(I)/FLOAT(NHIST)
    D0 910 I=1,NBIN
910  YST(I)=RAMAX*ZAMAX*SIGME*YST(I)/FLOAT(NHIST)
    THINCV=SUMNTH/SUMD
C
C
C    CALCULATE RANG(I),RTIME(I),T0TRAT,FT1 AND FT2
    D0 920 I=1,NANG
920  RANG(I)=YSA(I)/YDIR
    T0TRAT=0.0
    D0 1000 I=1,NBIN
    RTIME(I)=YST(I)/YDIR
1000  T0TRAT=T0TRAT+RTIME(I)
    FT2=RTIME(NBIN)/T0TRAT
    FT1=1.0-FT2
C
C
C    WRITE RESULTS
    WRITE(5,1900) YDIR
1900  FORMAT(4HYDIR/E10.4)
    WRITE(5,2000) TMIN,FREE
2000  FORMAT(9HTMIN,FREE/2E10.4)
    WRITE(5,2400)
2400  FORMAT(6HTHI(I))
    WRITE(5,3000) (THI(I),I=1,NANG)
    WRITE(5,2401)
2401  FORMAT(7HRANG(I))
    WRITE(5,3000) (RANG(I),I=1,NANG)
    WRITE(5,2001)
2001  FORMAT(4HT(I))
    WRITE(5,3000) (T(I),I=1,NTIME)
3000  FORMAT(4E10.4)
    WRITE(5,2002)
2002  FORMAT(8HRTIME(I))
    WRITE(5,3000) (RTIME(I),I=1,NBIN)

```

```

WRITE(5,2003) T0TRAT,FT1,FT2
2003 F0RMA1(14HT0TRAT,FT1,FT2/3E10.4)
WRITE(5,2004) THINCV
2004 F0RMA1(6HTHINCV/E10.4)
WRITE(5,2005)
2005 F0RMA1(/54-----)

```

C

```

G0 T0 1
END
FUNCTION TIME(EIN,H)
E=EIN/939.549
V=(+.2997925E+11)*SQRT(1.0-(1.0/(E+1.0)/(E+1.0)))
TIME=R/V
RETURN
END
SUBROUTINE ANGLE(X1H,Y1H,Z1H,X1T,Y1T,Z1T,X2H,Y2H,Z2H,X2T,Y2T,Z2T,
1H)
V1=SQRT((X1H-X1T)*(X1H-X1T)+(Y1H-Y1T)*(Y1H-Y1T)+(Z1H-Z1T)*(Z1H-Z1T))
V2=SQRT((X2H-X2T)*(X2H-X2T)+(Y2H-Y2T)*(Y2H-Y2T)+(Z2H-Z2T)*(Z2H-Z2T))
DOT=(X1H-X1T)*(X2H-X2T)+(Y1H-Y1T)*(Y2H-Y2T)+(Z1H-Z1T)*(Z2H-Z2T)
CTH=DOT/V1/V2
TH=ARCCOS(CTH,2)
RETURN
END
FUNCTION ARCCOS(X,K)
ARCCOS=1.5707963
IF(X*X.GT.1.0E-70) ARCCOS=ATAN(SQRT(1./X/X-1.))
IF(X.LT.0.) ARCCOS=3.1415926-ARCCOS
G0 T0 (100,200),K
100 ARCCOS=ARCCOS*57.2957795
200 RETURN
END
SUBROUTINE INTRPL(N,XT,YT,X,Y)
DIMENSION XT(N),YT(N)
IF(X-XT(1)) 1,3,4
1 WRITE(1,2)
2 F0RMA1(8HRANG ERR)
PAUSE
3 Y=YT(1)
G0 T0 24
4 IF(X-XT(N)) 7,5,1
5 Y=YT(N)
G0 T0 24
7 I=0
J=N
8 K=0.5*FL0AT(J-1)+0.1
K=K+I
IF(X-XT(K)) 9,10,11
9 J=K
G0 T0 12
10 Y=YT(K)
G0 T0 24
11 I=K
12 IF(J-I-1) 13,13,8
13 I=J
J=I-1
DEN=XT(J)-XT(I)
C1=(XT(J)*YT(I)-XT(I)*YT(J))/DEN

```

C2=(YT(J)-YT(I))/DEN

Y=C1+C2\*X

24 RETURN

END

5

## APPENDIX II

### Listing of FORTRAN IV Program AIRSC2

This program was used in conjunction with an SEL 840 MP computer equipped with an extended arithmetic unit to perform the calculations discussed in Section V. The interpolation tables included in the input provide basic physical data, such as cross sections, which are required for the calculations. Unit 1 refers to a teletype I/O device, Unit 4 is a card reader (or punch for output) while Unit 5 is a line printer.

C  
C  
AIRSC2

DIMENSION WS(5),ATHU(4),NUT(4),EUT(4,20),SIGUT(4,20),NUF(4),EUF(4,  
150),SIGUF(4,50),ENT(50),SIGNT(50),ENE(50),SIGNE(50),NWE(5),EWE(5  
2,30),WNE(5,30),QNI(3),NNI(3),ENI(3,20),SIGNI(3,20),EOT(50),SIGOT(5  
30),EOE(50),SIGOE(50),NWE(5),EWE(5,30),WOE(5,30),QOI(3),NOI(3),EO  
4I(3,20),SIGOI(3,20),T(20),YSCAT(21),RATIO(21),THIC(36),YSANG(36),F  
5ANG(36),ENER(100),YSEN(100),REN(100),A(50),B(50),WØRK(50)  
DATA ATMDN,ATMDØ,AVØG,PI1,PI2/.4034E+20,.1066E+20,.1E-23,3.14159,6  
1.28316/

C  
C  
C  
C  
VALUE(Z,VMIN,VMAX)=VMIN+Z\*(VMAX-VMIN)

CONTROL

1 READ(4,2) IC  
2 FØRMAT(I1)  
GØ TØ(10,20,30,40),IC  
10 PAUSE  
GØ TØ 1

C  
C  
C  
READ INTERPØLATION TABLES

20 DØ 22 I=1,4  
READ(4,21) NUT(I)  
21 FØRMAT(16I5)  
N=NUT(I)  
22 READ(4,23) (EUT(I,J),SIGUT(I,J),J=1,N)  
23 FØRMAT(8E10,4)  
DØ 231 I=1,4  
READ(4,21) NUF(I)  
N=NUF(I)  
231 READ(4,23) (EUF(I,J),SIGUF(I,J),J=1,N)  
READ(4,21) NNT  
READ(4,23) (ENT(I),SIGNT(I),I=1,NNT)  
READ(4,21) NNE  
READ(4,23) (ENE(I),SIGNE(I),I=1,NNE)  
DØ 24 I=1,5  
READ(4,21) NWE(I)  
N=NWE(I)  
24 READ(4,23) (EWE(I,J),WNE(I,J),J=1,N)  
READ(4,21) MNI  
IF(MNI.EQ.0) GØ TØ 26  
READ(4,23) (QNI(I),I=1,MNI)  
DØ 25 I=1,MNI  
READ(4,21) NNI(I)  
N=NNI(I)  
25 READ(4,23) (ENI(I,J),SIGNI(I,J),J=1,N)  
26 READ(4,21) NØT  
READ(4,23) (EØT(I),SIGØT(I),I=1,NØT)  
READ(4,21) NØE  
READ(4,23) (EOE(I),SIGOE(I),I=1,NØE)  
DØ 27 I=1,5  
READ(4,21) NWE(I)  
N=NWE(I)  
27 READ(4,23) (EWE(I,J),WØE(I,J),J=1,N)  
READ(4,21) MØI  
IF(MØI.EQ.0) GØ TØ 30  
READ(4,23) (QØI(I),I=1,MØI)

```

DØ 28 I=1,MØI
READ(4,21) NØI(I)
N=NØI(I)
28 READ(4,23) (EPI(I,J),SIGØI(I,J),J=1,N)

C
C
C
READ AND WRITE BASIC PARAMETERS

30 READ(4,21) MHIST,NHISTL,NTIME,NANG,NENR
READ(4,23) ZAMAX,RAMAX
READ(4,23) D,RDISK
READ(4,23) (ATMU(I),I=1,4)
READ(4,23) TRANG
READ(4,23) A1,A2,GS
WRITE(5,31) MHIST,NHISTL,NTIME,NANG,NENR
31 FØRMT(1H1,28HMHIST,NHISTL,NTIME,NANG,NENR/5I6)
WRITE(5,32) ZAMAX,RAMAX
32 FØRMT(11HZAMAX,RAMAX/2E10.4)
WRITE(5,33) D,RDISK
33 FØRMT(7HD,RDISK/2E10.4)
WRITE(5,34)
34 FØRMT(7HATMU(I))
WRITE(5,23) (ATMU(I),I=1,4)
WRITE(5,35) TRANG
35 FØRMT(5HTRANG/E10.4)
WRITE(5,36) A1,A2,GS
36 FØRMT(8HA1,A2,GS/3E10.4)
WRITE(5,37)
37 FØRMT(/5H.....)

C
C
C
READ AND WRITE VARIABLE PARAMETERS

40 READ(4,41) E1,NWS
41 FØRMT(E10.4,I5)
IF(NWS.GT.0) READ(4,23) (WS(I),I=1,NWS)
WRITE(5,42) E1,NWS
42 FØRMT(/6HE1,NWS/E10.4,I5)
IF(NWS.EQ.0) GØ TØ 50
WRITE(5,43)
43 FØRMT(5HWS(I))
WRITE(5,23) (WS(I),I=1,NWS)

C
C
C
CALCULATE T(I)

50 DØ 51 I=1,NTIME
51 T(I)=TRANG*FLØAT(I)/FLØAT(NTIME)

C
C
C
CALCULATE THIC(I)

DØ 52 I=1,NANG
52 THIC(I)=180.0*FLØAT(I)/FLØAT(NANG)

C
C
C
CALCULATE FLIGHT TIME SPREAD FØR DIRECT EVENTS,ENMAX AND ENER(I)

THS=ATAN(RDISK/D)
DØ=D/CØS(THS)
CALL KINAM(A1,A2,1.0087,GS,E1,THS,ENØ,EDUM)
TMAX=TIME(ENØ,DØ)
CALL KINAM(A1,A2,1.0087,GS,E1,0.0,ENØ,EDUM)
ENMAX=1.00001*ENØ
TMIN=TIME(ENØ,D)

```

```
DT=TMAX-TMIN
DØ 53 I=1,NENR
53 ENER(I)=ENMAX*FLØAT(I)/FLØAT(NENR)
```

```
C
C
C
CALCULATE ZERO-DEGREE MEAN FREE PATH
```

```
CALL INTRPL(NNT,ENT,SIGNT,ENO,VSNT)
CALL INTRPL(NØT,EØT,SIGØT,ENO,VSØT)
SIGAIR=AVØG*(ATMDN*VSNT+ATMDØ*VSØT)
FREE=1.0/SIGAIR
```

```
C
C
C
....CALCULATE YDIR
```

```
YDIR=0.0
DØ 100 IDIR=1,MHIST
```

```
C
C
C
SELECT RF AT RANDOM
```

```
Z=РАНF(-1)
RF=VALUE(Z,0.0,RDISK)
```

```
C
C
C
CALCULATE THS,DO AND ENO
```

```
THS=ATAN(RF/D)
CS=CØS(THS)
DØ=D/CS
CALL KINAM(A1,A2,1.0087,ØS,E1,THS,ENO,EDUM)
```

```
C
C
C
CALCULATE SOURCE FLUX
```

```
CALL DISTR(NWS,WS,THS,FS)
```

```
C
C
C
CALCULATE ATND
```

```
CALL INTRPL(NNT,ENT,SIGNT,ENO,VSNT)
CALL INTRPL(NØT,EØT,SIGØT,ENO,VSØT)
SIGAIR=AVØG*(ATMDN*VSNT+ATMDØ*VSØT)
ATTND=EXF(-SIGAIR*DO)
```

```
C
C
C
CALCULATE FUT AND FUF
```

```
FUT=0.0
DØ 61 I=1,4
N=NUT(I)
DØ 60 J=1,N
A(J)=EUT(I,J)
60 B(J)=SIGUT(I,J)
CALL INTRPL(N,A,B,ENO,VSUT)
61 FUT=FUT+ATMU(I)*VSUT
FUT=FUT*AVØG
FUF=0.0
DØ 63 I=1,4
N=NUF(I)
DØ 62 J=1,N
A(J)=EUF(I,J)
62 B(J)=SIGUF(I,J)
CALL INTRPL(N,A,B,ENO,VSUF)
63 FUF=FUF+ATMU(I)*VSUF
FUF=FUF*AVØG
```

```

C 100 YDIR=YDIR+(FS*CS*ATTNO*RF*FUF*TRANS(FUT,PI1,RDISK,CS)/DO/DO/FUT)
C
C CALCULATE HISTORY AVERAGE
C
C YDIR=YDIR/FLD*AT(MHIST)
C
C .....CALCULATE YSCAT(I),YSANG(I) AND YSEN(I)
C
C NBIN=NTIME+1
C D0 110 I=1,NBIN
110 YSCAT(I)=0.0
C D0 111 I=1,NANG
111 YSANG(I)=0.0
C D0 112 I=1,NENR
112 YSEN(I)=0.0
C SUMNE=0.0
C SUMNTH=0.0
C SUMD=0.0
C
C NHIST=0
113 CONTINUE
C NHIST=NHIST+1
C
C SELECT RF,RA,ZA AND PHA AT RANDOM
C
C Z=RANF(-1)
C RF=VALUE(Z,0.0,RDISK)
C Z=RANF(-1)
C RA=VALUE(Z,0.0,RA MAX)
C Z=RANF(-1)
C ZA=VALUE(Z,-ZAMAX,ZAMAX)
C Z=RANF(-1)
C PHA=VALUE(Z,0.0,PI2)
C
C CALCULATE XA,YA,D1 AND D2. SKIP TRIAL IF D1 OR D2 TOO SMALL
C
C XA=RA*COS(PHA)
C YA=RA*SIN(PHA)
C D1=SQRT(ABS(XA*XA+YA*YA+(ZA-D)*(ZA-D)))
C IF((D1/D)-.1E-05) 113,113,120
120 D2=SQRT(ABS((XA-RF)*(XA-RF)+YA*YA+ZA*ZA))
C IF((D2/D)-.1E-05) 113,113,130
C
C CALCULATE THS,EN1 AND T1
C
130 CALL ANGLE(0.,0.,0.,0.,0.,D,XA,YA,ZA,0.,0.,D,THS)
C CALL KINAM(A1,A2,1.0087,QS,E1,THS,EN1,EDUM)
C T1=TIME(EN1,D1)
C
C CALCULATE SOURCE FLUX
C
C CALL DISTR(NWS,WS,THS,FS)
C
C CALCULATE ATTN1
C
C CALL INTRPL(NNT,ENT,SIGNT,EN1,VSNT)
C CALL INTRPL(N0T,E0T,SIG0T,EN1,VS0T)
C SIGAIR=AV0G*(ATMDN*VSNT+ATMD0*VS0T)
C ATTN1=EXP(-SIGAIR*D1)
C

```

C  
C  
C  
CALCULATE THA,THI,THING AND JNDEX. SKIP TRIAL IF THING TOO CLOSE  
TO 90 DEGREES

CALL ANGLE(RF,C,,0,,XA,YA,ZA,XA,YA,ZA,D,,0,,D,THA)  
CALL ANGLE(0,,0,,0,,0,,0,,D,RF,0,,0,,XA,YA,ZA,THI)  
CI=ABS(COS(THI))  
THING=57.2957795\*THI  
IF(ABS(THING-90,0)=0.01) 113,113,131  
131 JNDEX=THING\*FLOAT(NANG)/180.001  
JNDEX=JNDEX+1

C  
CXX  
C  
C  
C  
CONTRIBUTION FROM NITROGEN ELASTIC SCATTERING

CALCULATE EN2,T2,INDEX AND KNDEX

CALL KINAM(1.0087,14.003,1.0087,0.,EN1,THA,EN2,EDUM)  
KNDEX=EN2\*FLOAT(NENR)/ENMAX  
KNDEX=KNDEX+1  
T2=TIME(EN2,D2)  
INDEX=(T1+T2-TMIN)\*FLOAT(NTIME)/TRANG  
INDEX=INDEX+1  
IF(INDEX.GT,NBIN) INDEX=NBIN

C  
C  
C  
C  
DETERMINE NORMALIZED NITROGEN DIFFERENTIAL ELASTIC SCATTERING  
CROSS SECTION

CALL INTRPL(NNE,ENE,SIGNE,EN1,VSNE)  
DØ 141 I=1,5  
N=NWNE(I)  
DØ 140 J=1,N  
A(J)=EWNE(I,J)  
140 B(J)=WNE(I,J)  
141 CALL INTRPL(N,A,B,EN1,WØRK(I))  
CALL NORM(WØRK,CØNST)  
CALL DISTR(5,WØRK,THA,S1)  
DESN=CØNST\*VSNE\*S1\*AVØG/PI2/2.0

C  
C  
C  
CALCULATE ATTN2

CALL INTRPL(NNT,ENT,SIGNT,EN2,VSNT)  
CALL INTRPL(NØT,EØT,SIGØT,EN2,VSØT)  
SIGAIR=AVØG\*(ATMDN\*VSNT+ATMDØ\*VSØT)  
ATTN2=EXP(-SIGAIR\*D2)

C  
C  
C  
CALCULATE FUT AND FUF

FUT=0.0  
DØ 151 I=1,4  
N=NUT(I)  
DØ 150 J=1,N  
A(J)=EUT(I,J)  
150 B(J)=SIGUT(I,J)  
CALL INTRPL(N,A,B,EN2,VSUT)  
151 FUT=FUT+ATMU(I)\*VSUT  
FUT=FUT\*AVØG  
FUF=0.0  
DØ 153 I=1,4  
N=NUF(I)  
DØ 152 J=1,N  
A(J)=EUF(I,J)

```

152 B(J)=SIGUF(I,J)
    CALL INTRPL(N,A,B,EN2,VSUF)
153 FUF=FUF+ATMU(I)*VSUF
    FUF=FUF*AVØG

```

```

C
YLD=FS*CI+ATTN1*ATTN2*RF*RA*ATMDN*DESN*FUF*TRANS(FUT,PI1,RDISK,CI
1/D1/D1/D2/D2/FUT
SUMNE=SUMNE+YLD*EN2
SUMNTH=SUMNTH+YLD*THINC
SUMD=SUMD+YLD
YSCAT(INDEX)=YSCAT(INDEX)+YLD
YSANG(JNDEX)=YSANG(JNDEX)+YLD
YSEN(KNDEX)=YSEN(KNDEX)+YLD

```

```

C
CXX CONTRIBUTION FROM NITROGEN INELASTIC SCATTERING
C

```

```

IF(MNI.EQ.0) GO TO 209
DØ 200 INI=1,MNI

```

```

C
C CHECK IF REACTION IS ENERGETICALLY ALLOWED. CALCULATE T2,INDEX
C AND KNDEX
C

```

```

CALL KINAM(1.0087,14.003,1.0087,QNI(INI),EN1,THA,EN2,EDUM)
IF(EN2) 200,200,160
160 T2=TIME(EN2,D2)
    KNDEX=EN2*FLØAT(NENR)/ENMAX
    KNDEX=KNDEX+1
    INDEX=(T1+T2-TMIN)*FLØAT(NTIME)/TRANG
    INDEX=INDEX+1
    IF(INDEX.GT.NBIN) INDEX=NBIN

```

```

C
C DETERMINE NORMALIZED NITROGEN DIFFERENTIAL INELASTIC SCATTERING
C CROSS SECTION (ISØTRØPIC)
C

```

```

N=NNI(INI)
DØ 161 J=1,N
A(J)=ENI(INI,J)
161 B(J)=SIGNI(INI,J)
    CALL INTRPL(N,A,B,EN1,VSNI)
    DISN=VSNI*AVØG/PI2/2.0

```

```

C
C CALCULATE ATTN2
C

```

```

CALL INTRPL(NAT,ENT,SIGNT,EN2,VSNT)
CALL INTRPL(NØT,EØT,SIGØT,EN2,VSØT)
SIGAIR=AVØG*(ATMDN*VSNT+ATMDØ*VSØT)
ATTN2=EXF(-SIGAIR*D2)

```

```

C
C CALCULATE FUT AND FUF
C

```

```

FUT=0.0
DØ 163 I=1,4
N=NUT(I)
DØ 162 J=1,N
A(J)=EUT(I,J)
162 B(J)=SIGUT(I,J)
    CALL INTRPL(N,A,B,EN2,VSUT)
163 FUT=FUT+ATMU(I)*VSUT
    FUT=FUT*AVØG
    FUF=0.0

```

```

D0 165 I=1,4
N=NUF(I)
D0 164 J=1,N
A(J)=EUF(I,J)
164 B(J)=SIGUF(I,J)
CALL INTRPL(N,A,B,EN2,VSUF)
165 FUF=FUF+ATMU(I)*VSUF
FUF=FUF*AV0G

```

C

```

YLD=FS*C I*ATTN1*ATTN2*RF*RA*ATMDN*DISN*FUF*TRANS(FUT,PI1,RDISK,CI)
1/D1/L1/D2/D2/FUT
SUMNE=SUMNE+YLD*EN2
SUMNTH=SUMNTH+YLD*THINC
SUMD=SUMD+YLD
YSCAT(INDEX)=YSCAT(INDEX)+YLD
YSANG(JNDEX)=YSANG(JNDEX)+YLD
YSEN(KNDEX)=YSEN(KNDEX)+YLD
200 CONTINUE

```

C

CXX CONTRIBUTION FROM OXYGEN ELASTIC SCATTERING

C

C

C

CALCULATE EN2,T2,INDEX AND KNDEX

```

.09 CALL KINAM(1.0067,15.995,1.0087,0.,EN1,THA,EN2,EDUM)
KNDEX=EN2*FLOAT(NENR)/ENMAX
KNDEX=KNDEX+1
T2=TIME(EN2,D2)
INDEX=(T1+T2-TMIN)*FLOAT(NTIME)/TRANG
INDEX=INDEX+1
IF(INDEX.GT.NBIN) INDEX=NBIN

```

C

C

C

DETERMINE NORMALIZED OXYGEN DIFFERENTIAL ELASTIC SCATTERING  
CROSS SECTION

```

CALL INTRPL(N0E,E0E,SIG0E,EN1,VS0E)
D0 211 I=1,5
N=NW0E(I)
D0 210 J=1,N
A(J)=EW0E(I,J)
210 B(J)=W0E(I,J)
211 CALL INTRPL(N,A,B,EN1,W0RK(I))
CALL NORM(W0RK,CNST)
CALL DISTR(5,W0RK,THA,S1)
DES0=CNST*VS0E*S1*AV0G/PI2/2.0

```

C

C

C

CALCULATE ATTN2

```

CALL INTRPL(NT,ENT,SIGNT,EN2,VSNT)
CALL INTRPL(N0T,E0T,SIG0T,EN2,VS0T)
SIGAIR=AV0G*(ATMDN*VSNT+ATMD0*VS0T)
ATTN2=EXF(-SIGAIR*D2)

```

C

C

C

CALCULATE FUT AND FUF

```

FUT=0.0
D0 221 I=1,4
N=NUT(I)
D0 220 J=1,N
A(J)=EUT(I,J)
220 B(J)=SIGUT(I,J)

```

```

221 CALL INTRPL(N,A,B,EN2,VSUT)
    FUT=FLT+ATMU(I)*VSUT
    FUT=FUT*AV0G
    FUF=0.0
    D0 223 I=1,4
    N=NUF(I)
    D0 222 J=1,N
    A(J)=EUF(I,J)
222 B(J)=SIGUF(I,J)
    CALL INTRPL(N,A,B,EN2,VSUF)
223 FUF=FUF+ATMU(I)*VSUF
    FUF=FUF*AV0G

```

C

```

YLD=FS*CI*ATTN1*ATTN2*RF*RA*ATMD0*DES0*FUF*TRANS(FUT,PI1,RDISK,CI)
1/D1/D1/D2/D2/FUT
SUMNE=SUMNE+YLD*EN2
SUMNTH=SUMNTH+YLD*THINC
SUMD=SUMD+YLD
YSCAT(INDEX)=YSCAT(INDEX)+YLD
YSANG(KINDEX)=YSANG(KINDEX)+YLD
YSEN(KINDEX)=YSEN(KINDEX)+YLD

```

C

CXx CONTRIBUTION FROM OXYGEN INELASTIC SCATTERING

C

```

IF(M01.EQ.0) GO TO 900
D0 300 I01=1,M01

```

C

C

C

C

CHECK IF REACTION IS ENERGETICALLY ALLOWED. CALCULATE T2,INDEX AND KINDEX

```

CALL KINAM(1.0087,15.995,1.0087,Q01(I01),EN1,THA,EN2,EDUM)
IF(EN2) 300,300,290
290 T2=TIME(EN2,D2)
    KINDEX=EN2*FLOAT(NENR)/ENMAX
    KINDEX=KINDEX+1
    INDEX=(T1+T2-TMIN)*FLOAT(ETIME)/TRANG
    INDEX=INDEX+1
    IF(INDEX.GT.NBIN) INDEX=NBIN

```

C

C

C

C

DETERMINE NORMALIZED OXYGEN DIFFERENTIAL INELASTIC SCATTERING CROSS SECTION (ISOTROPIC)

```

N=N01(I01)
D0 291 J=1,N
A(J)=E01(I01,J)
291 B(J)=SIG01(I01,J)
    CALL INTRPL(N,A,B,EN1,VS01)
    DIS0=VS01*AV0G/PI2/2.0

```

C

C

C

CALCULATE ATTN2

```

CALL INTRPL(NNT,ENT,SIGNT,EN2,VSNT)
CALL INTRPL(N0T,E0T,SIG0T,EN2,VS0T)
SIGAIR=AV0G*(ATMDN*VSNT+ATMD0*VS0T)
ATTN2=EXP(-SIGAIR*D2)

```

C

C

C

CALCULATE FUT AND FUF

```

FUT=0.0
D0 293 I=1,4

```

```

N=NUF(I)
DØ 292 J=1,N
A(J)=EUT(I,J)
292 B(J)=SIGUT(I,J)
CALL INTRPL(N,A,B,EN2,VSUT)
293 FUT=FUT+ATMU(I)*VSUT
FUT=FUT*AVØG
FUF=Ø,Ø
DØ 295 I=1,4
N=NUF(I)
DØ 294 J=1,N
A(J)=EUF(I,J)
294 B(J)=SIGUF(I,J)
CALL INTRPL(N,A,B,EN2,VSUF)
295 FUF=FUF+ATMU(I)*VSUF
FUF=FUF*AVØG

```

C

```

YLD=FS*CI+ATTN1*ATTN2*RF*RA*ATMDØ*DISØ*FUF*TRANS(FUT,PI1,RDISK,CI)
1/D1/D1/D2/D2/FUT
SUMNE=SUMNE+YLD*EN2
SUMNTH=SUMNTH+YLD*THING
SUMD=SUMD+YLD
YSCAT(INDEX)=YSCAT(INDEX)+YLD
YSANG(JINDEX)=YSANG(JINDEX)+YLD
YSEN(KINDEX)=YSEN(KINDEX)+YLD
900 CONTINUE

```

C

```

900 CONTINUE
CALL SSWTCH(1,K1)
IF(K1.EQ.1) GO TO 905
IF(NHIST-VHISTL) 113,905,905

```

C

C

C

C

C

C

CALCULATE HISTORY AVERAGES AND MULTIPLY BY AIR PARAMETER SPACE VOLUME

```

905 VØLU=2.Ø*RAMAX*ZAMAX*PI2
DØ 906 I=1,NANG
906 YSANG(I)=VØLU*YSANG(I)/FLØAT(NHIST)
DØ 907 I=1,NENR
907 YSEN(I)=VØLU*YSEN(I)/FLØAT(NHIST)
DØ 910 I=1,NBIN
910 YSCAT(I)=VØLU*YSCAT(I)/FLØAT(NHIST)

```

C

C

C

CALCULATE RATIO(I),RANG(I),REN(I),TØTRAT,FT1 AND FT2

```

TØTRAT=Ø.Ø
DØ 1000 I=1,NBIN
RATIO(I)=YSCAT(I)/YDIR
1000 TØTRAT=TØTRAT+RATIO(I)
DØ 1001 I=1,NANG
1001 RANG(I)=YSANG(I)/YDIR
DØ 1002 I=1,NENR
1002 REN(I)=YSEN(I)/YDIR
FT2=RATIO(NBIN)/TØTRAT
FT1=1.Ø-FT2

```

C

C

C

CALCULATE AVERAGE EN2 AND THINC

EN2V=SUMNE/SUMD  
THINCV=SUMNH/SUMD

C  
C  
C

WRITE RESULTS

```
WRITE(5,1900) YDIR
1900 FORMAT(4HYDIR/E10.4)
WRITE(5,2000) TMIN,DT,FREE
2000 FORMAT(12HTMIN,DT,FREE/3E10.4)
WRITE(5,2020) NHIST
2020 FORMAT(8HNHIST = ,I6)
WRITE(5,4000)
4000 FORMAT(7HENER(I))
WRITE(5,3000) (ENER(I),I=1,NENR)
WRITE(5,4001)
4001 FORMAT(6HREN(I))
WRITE(5,3000) (REN(I),I=1,NENR)
WRITE(5,4002)
4002 FORMAT(7HTHIC(I))
WRITE(5,3000) (THIC(I),I=1,NANG)
WRITE(5,4003)
4003 FORMAT(7HRANG(I))
WRITE(5,3000) (RANG(I),I=1,NANG)
WRITE(5,2001)
2001 FORMAT(4HT(I))
WRITE(5,3000) (T(I),I=1,NTIME)
3000 FORMAT(4E10.4)
WRITE(5,2002)
2002 FORMAT(8HRATIO(I))
WRITE(5,3000) (RATIO(I),I=1,NBIN)
WRITE(5,2003) T0TRAT,FT1,FT2
2003 FORMAT(14HT0TRAT,FT1,FT2/3E10.4)
WRITE(5,2004) EN2V,THINCV
2004 FORMAT(11HEN2V,THINCV/2E10.4)
WRITE(5,2005)
2005 FORMAT(/5H-----)
```

C

```
IF(K1.EQ.1) PAUSE
GO TO 1
END
FUNCTION TIME(EIN,R)
E=EIN/939.549
IF(E.GT.0.) GO TO 1
V=0.
GO TO 2
1 V=(+.2997925E+11)*SQRT(ABS(1.0-(1.0/(E+1.0)/(E+1.0))))
TIME=R/V
2 RETURN
END
SUBROUTINE KINAM(A1,A2,A3,Q,E1,TH3,E31,E32)
```

C

```
W1=931.473*A1
W2=931.473*A2
W3=931.473*A3
W4=W1+W2-W3-Q
EF=-Q*(1.0+(W1/W2)-(0.5*Q/W2))
EB=-Q*(1.0+(W1/(W2-W3))-(0.5*Q/(W2-W3)))
IF(E1-EF) 1,1,2
1 E31=0.0
11 E32=0.0
```

```

G0 T2 6
2 C=COS(T43)
A=2.0*(W3+W4+E1+Q)
B=2.0*E1*(W1-W4-Q)-(2.0*W4*Q+Q*Q)
D=E1*(E1+2.0*W1)*C*C
TERM=(B*B-2.0*W3*A*B+4.0*W3*W3*D)*E1*(E1+2.0*W1)
IF(TERM) 1,1,3
3 DEN=A*A-4.0*D
U=(4.0*W3*D-A*B)/DEN
V=2.0*C*SQRT(ABS(TERM))/DEN
E31=U+V
IF(E1-EB) 4,4,5
4 IF(TH3-1.5707963) 41,11,11
41 E32=U-V
G0 T2 6
5 E32=E31
6 RETURN
END
SUBROUTINE ANGLE(X1H,Y1H,Z1H,X1T,Y1T,Z1T,X2H,Y2H,Z2H,X2T,Y2T,Z2T,T
1H)
V1=SQRT(ABS((X1H-X1T)*(X1H-X1T)+(Y1H-Y1T)*(Y1H-Y1T)+(Z1H-Z1T)*(Z1H
1-Z1T)))
V2=SQRT(ABS((X2H-X2T)*(X2H-X2T)+(Y2H-Y2T)*(Y2H-Y2T)+(Z2H-Z2T)*(Z2H
1-Z2T)))
DOT=(X1H-X1T)*(X2H-X2T)+(Y1H-Y1T)*(Y2H-Y2T)+(Z1H-Z1T)*(Z2H-Z2T)
CTH=DOT/V1/V2
TH=ARCCOS(CTH,2)
RETURN
END
SUBROUTINE NORM(W,C)
DIMENSION W(5)
SUM=0.0
DO 1 I=1,36
TH=3.14159*FLMAT(I)/36.0
CALL DISTR(5,W,TH,S)
1 SUM=SUM+S*SIN(TH)
SUM=0.0872664*SUM
C=2.0/SUM
RETURN
END
SUBROUTINE DISTR(NW,W,TH,V)
DIMENSION W(5)
V=1.0
IF(NW,EO.C) G0 T2 4
DO 2 I=1,NW
2 V=V+W(I)*POLYL(2,I,TH)
IF(V) 3,4,4
3 V=0.0
4 RETURN
END
FUNCTION POLYL(IOP,N,ANGLE)
X = ANGLE
G0 T2(10,11,12), IOP
10 X = .017453293*X
11 X = COS(X)
12 NBIG = N-1
IF(NBIG) 1,2,3
1 POLYL = 1.0
G0 T2 100
2 POLYL = X

```

```

GØ TØ 100
3 PL = X
  PLM1 = 1.0
  DØ 4 L=1,NBIG
  PØLYL = (FLØAT(2*L+1)*X*PL - FLØAT(L)*PLM1)/FLØAT(L+1)
  PLM1 = PL
4 PL = PØLYL
100 RETURN
END
SUBROUTINE INTRPL(N,XT,YT,X,Y)
DIMENSION XT(N),YT(N)
IF(X=XT(1)) 1,3,4
1 WRITE(1,2)
2 FORMAT(8,HRANG ERR)
  PAUSE
3 Y=YT(1)
  GØ TØ 24
4 IF(X=XT(N)) 7,5,1
5 Y=YT(N)
  GØ TØ 24
7 I=0
  J=N
8 K=0.5*FLØAT(J-I)+0.1
  K=K+I
  IF(X=XT(K)) 9,10,11
9 J=K
  GØ TØ 12
10 Y=YT(K)
  GØ TØ 24
11 I=K
12 IF(J-I-1) 13,13,8
13 I=J
  J=I-1
  DEN=XT(J)-XT(I)
  C1=(XT(J)*YT(I)-XT(I)*YT(J))/DEN
  C2=(YT(J)-YT(I))/DEN
  Y=C1+C2*X
24 RETURN
END
FUNCTION ARCCØS(X,K)
ARCCØS=1.5707963
IF(ABS(X).GT.,999999) X=.999999*X/ABS(X)
IF(X*X.GT.1.0E-70) ARCCØS=ATAN(SQRT(ABS(1./X/X-1.)))
IF(X.LT.0.) ARCCØS=3.1415926-ARCCØS
GØ TØ (100,200),K
100 ARCCØS=ARCCØS*57.2957795
200 RETURN
END
FUNCTION TRANS(F,P,R,C)
V=F/P/R/R/C
IF(V-0.001) 1,1,2
1 TRANS=V-(0.5*V*V)
  GØ TØ 3
2 TRANS=1.0-EXF(-V)
3 RETURN
END
FUNCTION EXF(Z)
IF(Z) 1,1,3
1 IF(Z.LT.-70.0) Z=-70.0
  IF(Z.GT.-.1E-04) GØ TØ 2

```